Nonlinearity in the Pathway of El Niño–Southern Oscillation to the Tropical North Atlantic

JAKE W. CASSELMAN,[a] ANDRÉA S. TASCHETTO,[b,c] AND DANIELA I. V. DOMEISEN[a]

[a] *Institute for Atmospheric and Climate Science, ETH Zurich, Zurich, Switzerland*
[b] *Climate Change Research Centre, University of New South Wales, Sydney, New South Wales, Australia*
[c] *ARC Centre of Excellence for Climate Extremes, University of New South Wales, Sydney, New South Wales, Australia*

(Manuscript received 10 December 2020, in final form 17 May 2021)

ABSTRACT: El Niño–Southern Oscillation can influence the tropical North Atlantic (TNA), leading to anomalous sea surface temperatures (SSTs) at a lag of several months. Several mechanisms have been proposed to explain this teleconnection. These mechanisms include both tropical and extratropical pathways, contributing to anomalous trade winds and static stability over the TNA region. The TNA SST response to ENSO has been suggested to be nonlinear. Yet the overall linearity of the ENSO–TNA teleconnection via the two pathways remains unclear. Here we use reanalysis data to confirm that the SST anomaly (SSTA) in the TNA is nonlinear with respect to the strength of the SST forcing in the tropical Pacific, as further increases in El Niño magnitudes cease to create further increases of the TNA SSTA. We further show that the tropical pathway is more linear than the extratropical pathway by subdividing the interbasin connection into extratropical and tropical pathways. This is confirmed by a climate model participating in the CMIP5. The extratropical pathway is modulated by the North Atlantic Oscillation (NAO) and the location of the SSTA in the Pacific, but this modulation insufficiently explains the nonlinearity in TNA SSTA. As neither extratropical nor tropical pathways can explain the nonlinearity, this suggests that external factors are at play. Further analysis shows that the TNA SSTA is highly influenced by the preconditioning of the tropical Atlantic SST. This preconditioning is found to be associated with the NAO through SST-tripole patterns.

KEYWORDS: Dynamics; ENSO; Teleconnections; Tropical variability

1. Introduction

A well-known teleconnection originating from El Niño–Southern Oscillation (ENSO) is toward the tropical Atlantic. A positive sea surface temperature anomaly (SSTA) in the tropical Atlantic tends to follow an El Niño, while a negative SSTA can develop during La Niña events. The peak of this SSTA often lags ENSO's peak SST [December–February (DJF)] by one season, peaking between March and May (MAM) (Enfield and Mayer 1997; Lee et al. 2008). The SSTA response occurs principally in the tropical North Atlantic (TNA) and is diminished south of the equator. Several reasons have been proposed for this hemispherical difference, including the lack of significant convection in the South Atlantic (Chiang and Sobel 2002), the meridional position of the intertropical convergence zone (ITCZ) (Czaja et al. 2002), opposing impacts of trade winds on either side of the equator (Wu et al. 2005), and the presence of destructive interference in the more dynamically responsive South Atlantic Ocean (Chang et al. 2006).

The TNA region, and associated SST anomalies, are noteworthy as they can influence several regions. Some examples include shifts in the ITCZ that can influence South America's rainfall (Nobre and Shukla 1996; Giannini et al. 2004; Rodrigues et al. 2011), or modulation of the ENSO teleconnections toward Europe (Mathieu et al. 2004). The North Atlantic Oscillation (NAO) may also be influenced by North Atlantic SSTs, of which subtropical SSTs represent the largest influence (Sutton et al. 2000; Robinson et al. 2003). Caribbean precipitation can be influenced by modifying the zonal SST gradient between the Atlantic and the Pacific, altering the Caribbean low-level jet (CLLJ) (Whyte et al. 2008; Mc Shine et al. 2019). The TNA region also impacts Atlantic hurricane activity by influencing the Atlantic warm pool (Wang et al. 2006; Vimont and Kossin 2007). Remote regions can also be impacted, including surface temperatures over China (Wu et al. 2011).

Different mechanisms have been proposed that connect the Pacific and Atlantic via the tropics (Saravanan and Chang 2000; Chang et al. 2006; Sasaki et al. 2014a; García-Serrano et al. 2017), extratropics (Lau and Nath 1996; Nobre and Shukla 1996; Alexander et al. 2002), or a combination of tropical and extratropical pathways (Huang 2002; Rodrigues et al. 2011; Taschetto et al. 2016; Jiang and Li 2019). Each mechanism can contribute to the TNA SST anomalies by creating latent heat changes via either a moist convection/stability process or a modification of the trade winds, with the latter strongly dominating over the former (Jiang and Li 2019). These anomalous trade winds often peak 1–2 months prior to the peak Atlantic SSTA, occurring between January and March (JFM). Furthermore, the coupling between the winds and underlying SST varies with latitude.

In addition to the TNA SST being forced by ENSO, the NAO may also influence the TNA region. The Azores high (southern lobe of the NAO) can modify the pressure gradient between

Supplemental information related to this paper is available at the Journals Online website: https://doi.org/10.1175/JCLI-D-20-0952.s1.

Corresponding author: Jake William Casselman, cjake@ethz.ch

Publisher's Note: This article was revised on 1 September 2021 to include a better resolution version of Fig. 2.

DOI: 10.1175/JCLI-D-20-0952.1

the Atlantic subtropics and the TNA, leading to anomalous trade winds and changes in heat fluxes and SST (Cassou and Terray 2001; George and Saunders 2001; Wanner et al. 2001; Lee et al. 2008). Consequently, the NAO is associated with a North Atlantic SST tripole pattern, of which the southernmost area overlaps with the TNA (Czaja et al. 2002). The NAO can be constructive or destructive to the influence of ENSO on the tropical Atlantic. The resulting interaction is further complicated as ENSO can also influence the NAO through the extratropical pathway (Jiménez-Esteve and Domeisen 2018).

Following an ENSO event or a large anomaly in the NAO index, peak trade wind anomalies occur between 20° and 30°N, where the SSTA persistence is related primarily to the forcing persistence (NAO or ENSO) (Czaja et al. 2002). Between 10°N and the equator, the wind–evaporation–SST (WES) feedback is important for generating and sustaining the SSTA in the TNA (Amaya et al. 2017; Xie and Philander 1994). As the TNA is typically warmer (colder) during El Niño (La Niña), this inhibits the southward excursion of the ITCZ during MAM. The ITCZ migration is also associated with the interhemispheric flow, further influencing the trade winds. The flow of surface winds toward the warm anomaly can create an SSTA dipole about the equator (Giannini et al. 2004; Wu et al. 2005), generating an SST pattern similar to the Atlantic meridional mode (Servain et al. 1999; Chiang and Vimont 2004).

The ENSO extratropical pathway toward the TNA explains approximately two-thirds of trade wind anomalies over the TNA region (Jiang and Li 2019). This influence occurs primarily through the Pacific–North American (PNA) pattern. The PNA is a wave train of alternating highs and lows arching from the tropical Pacific toward North America (Wallace and Gutzler 1981). The low-pressure center over the southeastern United States and the Caribbean is important for this teleconnection, influencing the TNA trade winds by interacting with the Azores high (Taschetto et al. 2016).

El Niño (La Niña) events tend to project onto a positive (negative) phase of the PNA (Horel and Wallace 1981). During El Niño events, the Aleutian low usually deepens and shifts southward, resulting in a strengthening and eastward extension of the subtropical jet (Cassou and Terray 2001; Brönnimann 2007). During La Niña events, the opposite influence generally occurs, except that a strengthening of the Aleutian low is nonlinear with the magnitude of the event (Straus and Shukla 2002). This nonlinearity originates from nonlinearities in the relationship between SSTs and convection over the tropical Pacific (Jiménez-Esteve and Domeisen 2019). A second trough located over the southeastern United States and Caribbean region is more linear to the strength of ENSO (Maldonado et al. 2016). This region is important for developing the TNA SSTA, as it can influence the downward motion of air in the Atlantic subtropical high (Hastenrath 2000). During El Niño events, the positive PNA creates an anomalous low pressure center around southeastern North America/tropical North Atlantic that weakens the equatorward flank of the subtropical high, contributing to a decrease in the Atlantic trade winds (Taschetto et al. 2016). This region can be further influenced by an anomalous Hadley circulation over the Atlantic, perturbed by the Walker circulation (Wang 2004).

Tropical teleconnections have also been proposed for the Pacific's influence on the Atlantic, influencing trade winds and static stability over the Atlantic. The tropical pathway is suggested to account for approximately one-third of the wind anomalies in the TNA region (Jiang and Li 2019). A commonality between the tropical mechanisms is the Matsuno–Gill-type response over the Pacific SST anomalies, linked to the propagation of Kelvin waves. Differences in wave propagation may arise between El Niño and La Niña events, which can create nonlinearities downstream (Lin et al. 2007). These differences originate from several aspects and are not well understood.

The first tropical mechanism involves warming the free troposphere over the Pacific, following convective adjustment to the SST anomalies, referred to as the "tropospheric temperature (TT) mechanism" (Sobel et al. 2002). This temperature anomaly propagates eastward via the aforementioned Kelvin wave, eventually encompassing much of the global tropical troposphere (Chiang and Sobel 2002). Su et al. (2003) found that this mechanism is linear as it operates over large areas. This finding is consistent with Lin et al. (2007), who found that the differences in convergent/divergent anomalies between El Niño and La Niña have little influence on the downstream temperature anomaly. Over the Atlantic, this mechanism influences the TNA SST by altering static stability, which alters deep convection. As a result, evaporative cooling anomalies and shortwave radiation changes can create SST anomalies (Klein et al. 1999; Chiang and Sobel 2002).

As the Kelvin wave propagates to the Atlantic, it influences the Hadley and Walker circulations, resulting in increased (decreased) upper-level westerlies during El Niño (La Niña) events and thus increasing (decreasing) the vertical wind shear and inhibiting (promoting) deep convection over South America and the tropical Atlantic (Sasaki et al. 2014a; Saravanan and Chang 2000). A recently discovered mechanism by García-Serrano et al. (2017) involves a secondary Gill-type response downstream of the tropical Pacific, with an anomalous heat source over the Amazon. This response is related to a perturbed Walker circulation and has the opposite sign of the Pacific's initial Matsuno–Gill response. During El Niño (La Niña) events, this response corresponds to anomalous descending (ascending) motion over South America and anticyclonic (cyclonic) activity at the surface. Similar to the perturbed ITCZ, this influences the trade winds in the deep tropics, with the TNA trade winds decreasing (increase) during El Niño (La Niña), helping to establish the WES feedback (Czaja et al. 2002).

In addition to different pathways for the teleconnection, other aspects of ENSO influence this teleconnection. For example, the rate that Pacific SST anomalies dissipate plays a role in the evolution of the TNA SST (Lee et al. 2008). A slower decay of ENSO often corresponds to a larger and earlier peak of TNA SSTA (Wu and He 2019; Wu et al. 2020). The longitudinal variance of Pacific SST anomalies during El Niño and ENSO diversity also plays an important role,

TABLE 1. Summary of events considered for moderate, strong, and extreme events. Years refer to the peak and decay year of each ENSO event.

Phase	Moderate	Strong	Extreme
El Niño	1963/64, 1968/69, 1969/70, 1976/77, 1977/78, 1986/87, 1987/88, 1994/95, 2004/05, 2006/07, 2014/15, 2018/19	1965/66, 1972/73, 1991/92, 2002/03, 2009/10	1982/83, 1997/98, 2015/16
La Niña	1961/62, 1962/63, 1964/65, 1967/68, 1971/72, 1974/75, 1983/84, 1984/85, 1995/96, 2000/01, 2008/09, 2011/12, 2016/17, 2017/18	1970/71, 1973/74, 1975/76, 1988/89, 1998/99, 1999/2000, 2007/08, 2010/11	—

where the position of the SSTA may modify aspects of the teleconnection pathways (Graf and Zanchettin 2012; Amaya and Foltz 2014; Taschetto et al. 2016; Zhang et al. 2019). Aside from ENSO considerations, the preconditioning of the tropical Atlantic SST, before establishing the teleconnection, can modify the SST by reinforcing or reducing the response (Giannini et al. 2004).

Overall, the complexity of the direct forcing from ENSO and other aspects like the NAO forcing or Atlantic SST preconditioning makes this interbasin connection nontrivial. This teleconnection's overall linearity remains unclear, as some studies have pointed to strong ENSO events not always resulting in a strong TNA SSTA (Lee et al. 2008; Wu et al. 2020). This is because many studies have often performed either a linear regression (Klein et al. 1999; Chiang and Sobel 2002; Saravanan and Chang 2000; Sasaki et al. 2014b; García-Serrano et al. 2017) or considered only one phase of ENSO (Yulaeva and Wallace 1994; Sobel et al. 2002; Su et al. 2003; Chiang and Lintner 2005; Rodrigues and McPhaden 2014; Taschetto et al. 2016). Here, we focus on analyzing the linearity of this teleconnection through both tropical and extratropical pathways and during both phases of ENSO.

2. Data and methods

This study uses the monthly mean SST from the Extended Reconstructed Sea Surface Temperature (ERSST), version 4, dataset (Huang et al. 2015), and atmospheric fields from the Japanese 55-year Reanalysis (JRA-55) (Kobayashi et al. 2015), both from January 1958 until December 2019. A 30-yr filter was used to remove the low-frequency variability in all fields using a fast Fourier transform (FFT). Results using filtered data were very similar to raw data. ENSO events are classified using the normalized ERSST dataset with a 5-month running average applied. ENSO events are defined using the October–February (ONDJF) Niño-3.4 index, defined by an area average encompassing the equatorial Pacific (5°N–5°S, 170°–120°W). Moderate events are defined as ±0.5–1.0 standard deviation (std dev), strong events as ±1.0–2.0 std dev, and extreme events as greater than ±2.0 std dev. This classification yields 12 moderate, 5 strong, and 3 extreme El Niño events, and 14 moderate, 8 strong, and 0 extreme La Niña events (see Table 1 for specific years). The statistical significance is calculated using a Monte Carlo test (Noreen 1990) by drawing a number of samples equal to the number of available events for each ENSO category from the full dataset. This procedure is repeated 10 000 times to determine significance.

We utilize 500 years from the Geophysical Fluid Dynamics Laboratory (GFDL) Climate Model, version 3 (CM3), preindustrial phase 5 of the Coupled Model Intercomparison Project (CMIP5) run. We choose this model due to its good representation of ENSO characteristics (Taschetto et al. 2014; Feng et al. 2020) and large-scale teleconnection patterns (Lee et al. 2014).

ENSO's impact onto the TNA SST is measured using a TNA index defined as the area-averaged SSTA over the region of 5°–25°N, 55°–15°W, as in Taschetto et al. (2016). The PNA pattern is represented using the first EOF of the 200 hPa geopotential height anomaly over 20°–80°N, 210°–30°W (as outlined by Straus and Shukla 2002). A $\sqrt{\cos\phi}$ weighting was applied before performing the EOF analysis, where ϕ is latitude.

The southeastern low pressure section of the PNA is analyzed independently, given its importance for influencing the Azores high and Atlantic trade winds. We define the southeastern index as the sea level pressure (SLP) averaged over 25°–35°N, 90°–70°W, referring to the trough located over the southeastern United States. The longitudinal variance of ENSO is measured by using the El Niño Modoki index (EMI) (Ashok et al. 2007).

For the NAO, we use the index by Li and Wang (2003) measuring the difference between the zonally averaged SLP at 35° and 65°N from 80°W to 30°E. We choose this index over an EOF analysis as it explains a larger percentage of variance in boreal spring and summer.

Two indices represent the tropical teleconnection pathways, referred to as the TT index and the secondary Gill index. Both patterns refer to a Kelvin wave perturbation but influence the tropical North Atlantic through two mechanisms. The TT mechanism primarily influences the Atlantic's stability by inhibiting moist convection, while the secondary Gill mechanism acts directly onto the trade winds over the Atlantic. The secondary Gill index is called after the mechanism by García-Serrano et al. (2017) and should not be mistaken for a separate mechanism from the initial Matsuno–Gill response occurring over the Pacific. We here refer to "secondary" as the downstream effect of the same phenomenon.

The TT index measures the average temperature anomaly between 850 and 200 hPa over the tropical Atlantic (5°N–5°S, 70°–10°W), as defined in Amaya and Foltz (2014). To represent the downstream perturbation of the Walker circulation, which results in a vertical shear anomaly and secondary Gill-type

response, we use the first mode of a maximum covariance analysis (MCA) between the Pacific SST over 45°N–45°S, 240°–60°W and the tropical Atlantic 200 hPa streamfunction over 30°N–30°S, 90°W–45°E. Before calculating the streamfunction, zonal means of each wind component are removed, creating the asymmetric streamfunction component. The MCA is constructed by computing a covariance matrix between the two datasets, then a singular value decomposition is used to determine the dominant modes of covariability, as described by Bretherton et al. (1992). By correlating the temporal expansion coefficients of a given variable for the nth MCA mode with the corresponding anomaly field, we form homogeneous maps (Barreto et al. 2017; Riaz et al. 2018). The first MCA between the Pacific SST and Atlantic 200 hPa asymmetric streamfunction represents 89% of covariance (Figs. 1b,c).

To evaluate each index's linearity, we separate ENSO events into moderate, strong, and extreme bin ranges, as well as a rolling ONDJF Niño-3.4 range. We use bins with a width of 0.5 std dev and shift the endpoints incrementally by 0.1 std dev, starting at −2.0 to −1.5 std dev, then −1.9 to −1.4 std dev, and so on. Furthermore, the mean, standard deviation, and coefficients of determination (R^2) were computed for each bin. We determine the extent that each index approximates a linear fit using an ordinary least squares method on all binned values. A shifting bin method is similar to performing a simple correlation between two indices, but by binning, we can determine additional aspects such as the mean and standard deviation. (For reference, we also include the corresponding scatterplots that do not use the aforementioned binning method in the Figs. S1 and S2 in the online supplemental material.) Note that when using the shifting bin method, events fall within multiple bins.

In addition to using the rolling ONDJF Niño-3.4 binning process with individual indices, we utilize this binning process on the standardized SST anomalies over the tropical Atlantic. To determine the deviation from the linear fit, a root-mean-squared error (RMSE) between the binned values and the linear fit is computed as

$$\mathrm{RMSE} = \sqrt{\frac{1}{n}\sum_{i=1}^{n}(y_i - \hat{y}_i)^2} \tag{1}$$

where y_i is the observed value and $\hat{y}_i$ is the value predicted by the linear regression, each for the ith value.

To quantify the interaction between the ITCZ and the meridional winds, we use an MCA between the precipitation and 950 hPa meridional winds. To determine the tropospheric stability, we calculate the lower-tropospheric stability (LTS) field defined as the difference in the potential temperature (θ) between 700 hPa and the surface, assumed to be 1000 hPa (Klein and Hartmann 1993; Wood and Bretherton 2006):

$$\mathrm{LTS} = \theta_{700} - \theta_{1000} \tag{2}$$

All aforementioned indices are summarized in Fig. 1a.

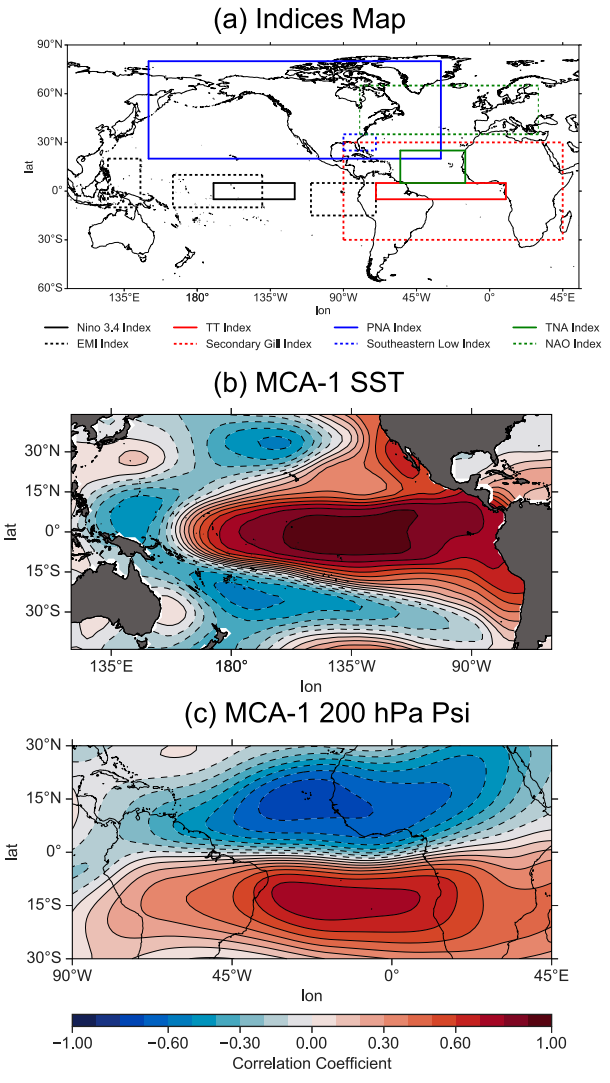

FIG. 1. (a) Indices map depicting the regions used to construct indices throughout this paper, including the Niño-3.4 (solid black lines), EMI (dashed black lines), TT index (solid red lines), secondary Gill index (dashed red lines), PNA index (solid blue lines), southeastern low index (dashed blue), TNA index (solid green line), and NAO (dashed green lines). (b),(c) The secondary Gill-type index MCA, where (b) is the SST over the Pacific and (c) is the 200 hPa streamfunction over the tropical Atlantic.

3. Results

a. *Tropical Atlantic connection*

We begin by compositing the TNA SST, SLP, and 950 hPa wind anomalies during JFM and MAM ENSO events (Fig. 2). We composite events for moderate, strong, and extreme ENSO events over the Atlantic. Note that the extreme ENSO composite only contains El Niño events.

The SST spatial patterns for La Niña and El Niño events show differences. For example, the spatial pattern during moderate La Niña (Fig. 2b) shows similarity in the spatial

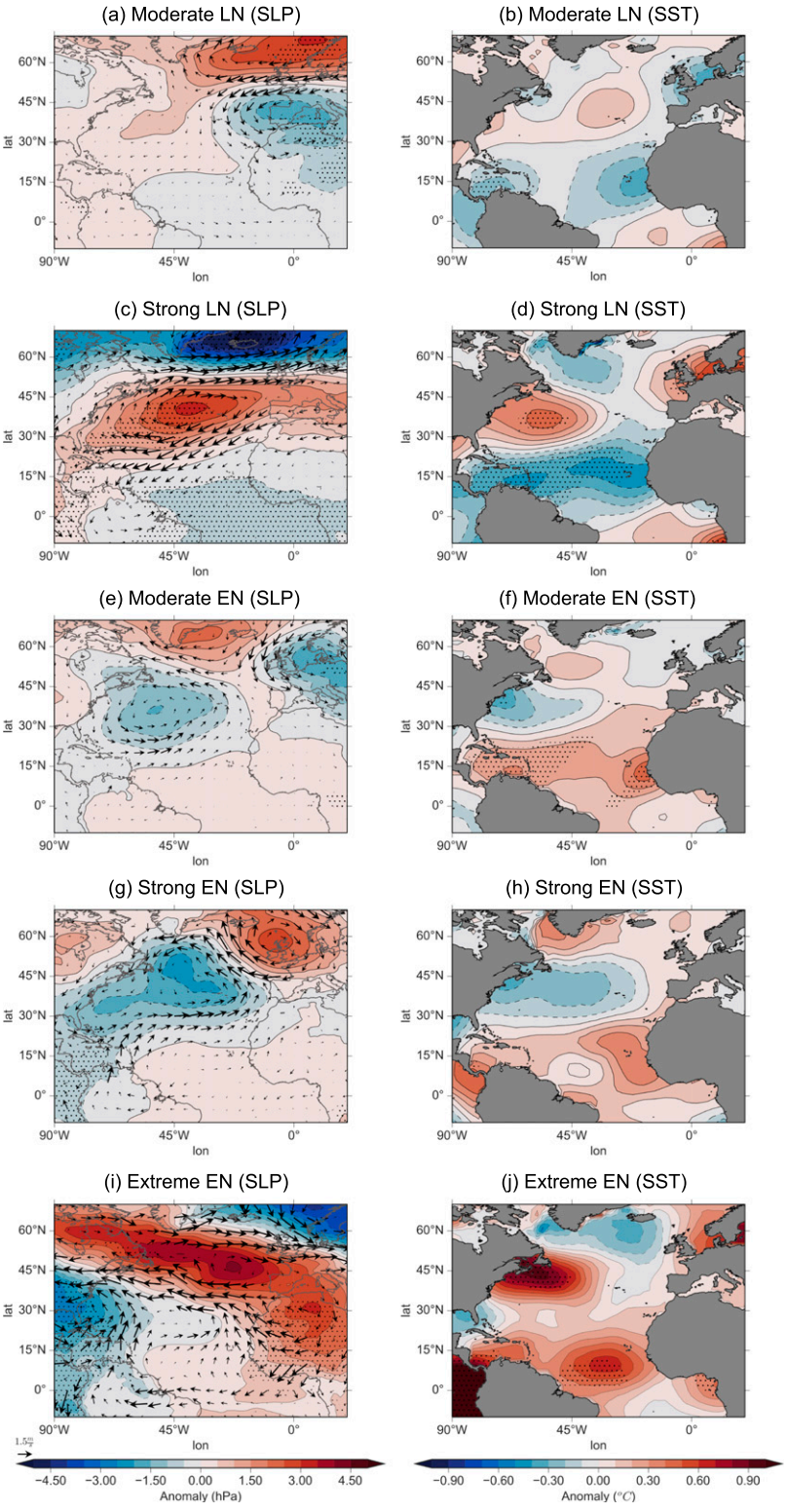

FIG. 2. Tropical Atlantic SST, SLP, and 950 hPa wind anomalies during ENSO: (right) the Atlantic SST in MAM, following a moderate, strong, and extreme El Niño and La Niña events; (left) the JFM SLP and 950 hPa wind vectors. Stippling represents areas that are statistically significant from zero at the 95% level using a two-tailed Monte Carlo test.

distribution of the TNA between 20°N and 0° to the strong El Niño event (Fig. 2h), as anomalies peak in the Caribbean and easternmost TNA regions. In contrast, the moderate El Niño (Fig. 2f) spatial distribution is similar to the strong La Niña (Fig. 2d), as the SST anomalies are more zonally symmetric. The extreme El Niño composite (Fig. 2j) shows different SSTA patterns, as the significant SST anomalies are primarily constrained to the deep tropics and Caribbean region.

Strong La Niña events show stronger anomalies in the central TNA region and the Caribbean while increasing slightly in the eastern TNA compared to moderate La Niña. Strong El Niño events show little increase in strength in the TNA with respect to moderate El Niño events and have a smaller extent of SST anomalies. A Monte Carlo analysis indicates that strong El Niño events lack statistical difference to moderate El Niño, while extreme El Niño events are only statistically different to moderate El Niño events in the deep tropics (Fig. S3).

The lack of SST differences between moderate and strong El Niño events contrasts with the large differences in wind anomalies at 20°N (typical peak wind area). Furthermore, the wind differences between moderate La Niña and El Niño events (Figs. 2a,e) show El Niño events are associated with a stronger anomaly over the TNA region, especially around 20°N. To expand on this, we analyze anomalies in the subtropical high region in the Atlantic, as variations in the semipermanent pressure center affect the trade wind anomalies during JFM (Figs. 2a,c,e,g,i). Both moderate El Niño and La Niña are associated with a negative NAO (Figs. 2a,e), though with a stronger signature over the eastern North Atlantic for La Niña, while the signature encompasses much of the North Atlantic for El Niño. The influence of a negative NAO would be constructive to the expected El Niño TNA wind anomaly, while destructive to the expected La Niña wind anomaly. This could explain the lack of strong trade wind anomalies at 20°N during moderate La Niña, as well as the lack of strong SSTA. Areas with significant SSTA hint at tropospheric stability changes (see also Fig. S4).

When considering the extratropical pathway, for El Niño (La Niña), the PNA is often in a positive (negative) phase; therefore, we expect a low (high) pressure anomaly over the western Atlantic and the United States. This signature is approximately what we see for all composites (Figs. 2a,c,e,g,i). The positive pressure anomaly over the western Atlantic could explain why the trade wind anomalies during moderate La Niña events still increase in strength, even as the negative NAO tends to force the trade winds to decrease. Furthermore, since the southern lobe of the NAO signature for moderate La Niña does not extend as far south as for strong La Niña, the peak anomaly lies further northward, having a smaller influence on the subtropical SST. This brings to light the importance of considering both the wind magnitude and position for explaining the lack of SST anomalies in the central TNA during moderate La Niña. A similar SST pattern is present during strong El Niño events, where strong trade wind anomalies are present, but peak north of 15°N. This may similarly explain the lack of SSTA, especially south of 15°N.

Strong La Niña and El Niño events exhibit similar NAO magnitudes (Figs. 2c,g), with opposite phases, and are constructive to the expected trade wind anomalies for both La Niña and El Niño. Even as the NAO pattern for strong El Niño is tilted more in the southwest–northeast direction, and the La Niña has a more north–south orientation, the wind anomalies over the TNA region are similar in position and strength. However, this results in a different SSTA pattern, indicating the magnitude of the trade wind anomaly is not the only factor to consider. Other factors may include wind anomaly location, as well as the background state, especially the preconditioning of the SST. Finally, the extreme El Niño composite shows distinct wind anomalies. This includes weaker winds in the central Atlantic around 20°N and stronger winds in the eastern and western TNA. The dominant SLP gradient also shifts from primarily meridional to primarily zonal. This may explain the different trade wind anomalies, as the meridional component of the TNA wind anomalies has increased. The only statistically different region compared to moderate El Niño is 0°–10°N (Fig. S3b), which may indicate that the extratropical pathway was not dominant, resulting in the tropical pathway dominating the TNA SSTA. However, as there are only three extreme events, these results should be taken with caution.

b. *Tropical Atlantic nonlinearity*

We plot the seasonal evolution of the Niño-3.4 and the TNA indices for each binned range (Figs. 3a,b). The Niño-3.4 index (Fig. 3a) shows a linear increase in strength as ENSO magnitude increases. As expected, the TNA's peak SSTA occurs approximately during MAM (Fig. 3b). Furthermore, the La Niña years show a linear increase in TNA SSTA from moderate to strong events. In contrast, during El Niño events, the TNA SSTA do not show a linear increase, as moderate and strong events have similar peak SSTA. Another difference occurs between the TNA SST's preconditioning, where strong El Niño events have the smallest SSTA in boreal winter. This difference may explain why the SSTA is similar between moderate and strong El Niño.

By considering only the TNA SSTA peak season (MAM) (Fig. 3c) and moving from strong La Niña to extreme El Niño events, we can better understand this relationship. Results show a linear relationship between ENSO and the TNA for La Niña events, as the mean resembles the linear fit (dashed line). This relationship changes for El Niño events, where further increases past 1.0–1.5 Niño-3.4 std dev result in a minimal increase in the TNA SSTA. Of this increase, a large percentage likely originates from the deep tropics, as this is the only region that increases between strong and extreme El Niño composites. This indicates a nonlinearity between ENSO's strength and the resulting TNA SST, although the low number of extreme El Niño makes it hard to show statistical significance. Since the TNA index provides little information about the spatial distribution of relative linearity, we compute the deviation from the linear fit for each grid point.

Figures 4a, 4c, and 4e shows the RMSE following a pointwise regression analysis between the Niño-3.4 index (ONDJF) and the normalized Atlantic SST anomalies between March and May. Since we normalize to background variability, this analysis shows the relative linearity between different regions within the TNA region. Results show higher linearity (lower

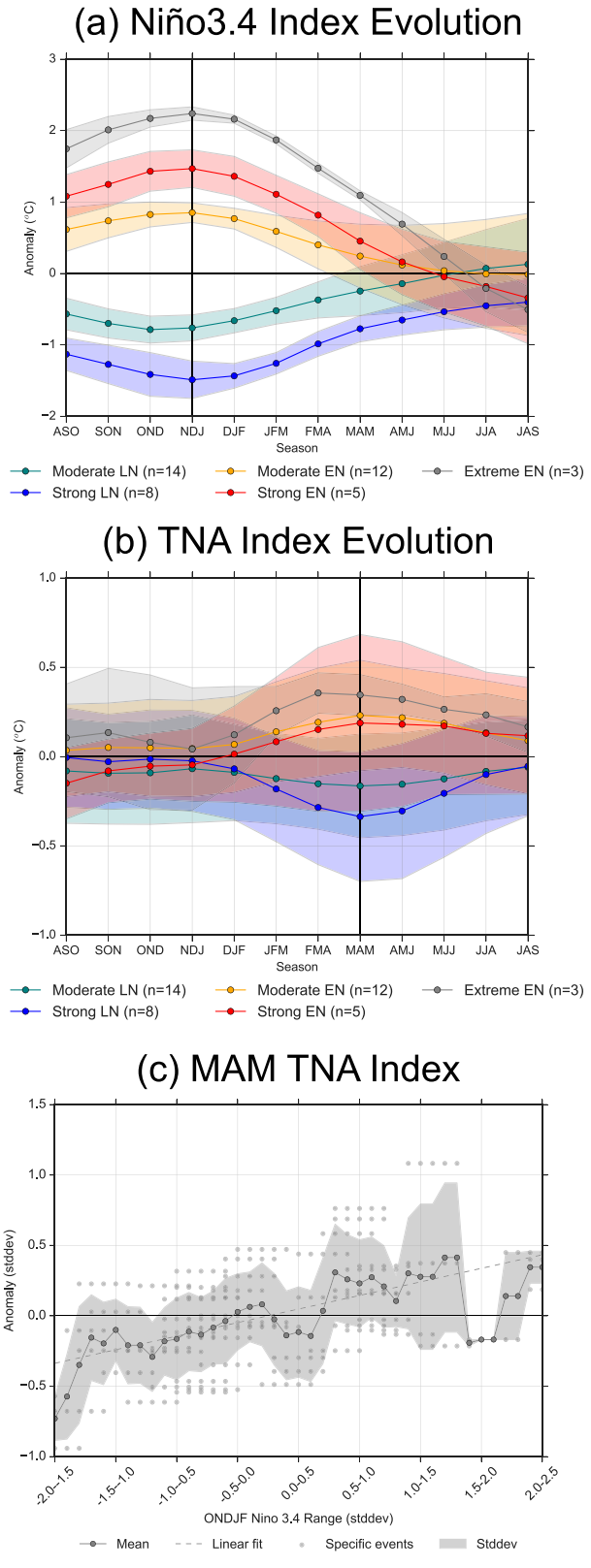

FIG. 3. Composited seasonal evolution chart. The seasonal (3-month running) average for (a) the Niño-3.4 index and (b) the TNA index. Each index is divided into El Niño (EN) and La Niña (LN) events, as well as by strength into moderate (±0.5–1.0 std dev), strong (±1.0–2.0 std dev) and extreme (>± 2.0 std dev) using the ONDFJ Niño-3.4 index. Shading represents ±1 std dev, while vertical line indicates peak season. (c) The TNA SSTA during MAM (peak month) and varying the ONDFJ Niño-3.4 range. Bins are 0.5 std dev wide and increase incrementally by 0.1 std dev. Shading represents ±1.0 std dev, solid scatter points represent the mean, faded scatter points represent individual events, and the straight line represents a best fit (using a least squares method). The sudden disappearance of the std dev (shaded) area in (c) is due to one value being available for the given bin.

RMSE indicates higher linearity, that is, smaller deviation from a linear fit) within the Caribbean region, and in the deep tropics between 0° and 15°N. The latitudinal band of relatively low RMSE extends from the northern coast of South America, growing slightly from March to April, before receding in May. The deep tropics RMSE values grow continuously from March to May, and two centers develop about the equator by May.

Compared to the SST composites in Fig. 2, the higher linearity found in the Caribbean (Figs. 4a,c,e) is consistent with the moderate, strong, and extreme bins of ENSO. In comparison to the location of peak wind anomalies, the low RMSE in the Caribbean occurs in a different area to the wind anomalies. This may indicate areas showing higher linearity (i.e., Caribbean and deep tropics) are more strongly associated with static stability processes linked to the tropical pathway, specifically the TT mechanism. This is consistent with Chiang and Sobel (2002), who found that the SST response to the TT mechanism is relatively weak in areas that are weakly coupled to the atmosphere. The weak response arises from a lack of communication between the free troposphere and the boundary layer through convection.

To analyze areas where the SST can be influenced by static stability changes (i.e., coupled to the atmosphere) or trade wind changes, we implement a multiple linear regression (MLR) (Figs. 4b,d,f). This method accounts for the variance associated with each variable, similar to the method implemented in Izumo et al. (2010). We use the LTS, which compares potential temperature at the surface to the potential temperature above the trade wind inversion, as outlined by Klein and Hartmann (1993), as well as the 950 hPa wind magnitudes. The LTS better quantifies large-scale stability changes, as variations in potential temperature above the trade wind inversion are related to the tropics, including distant convective regions (Miller 1997). No lag was used between the fields. Results are qualitatively similar when using JFM for wind and stability fields versus MAM SSTA.

We examine the multicollinearity between the stability and 950 hPa winds by considering the variance inflation factor (VIF), which is $1/(1-R^2)$. This analysis shows that the stability and 950 hPa winds have a low VIF, indicating that the explanatory variables are sufficiently unrelated, thus justifying the use of MLR analysis. Figure 4b shows that the trade winds' influence onto the SST peaks over the central TNA region around 20°N, diminishing into the Caribbean. Conversely, the

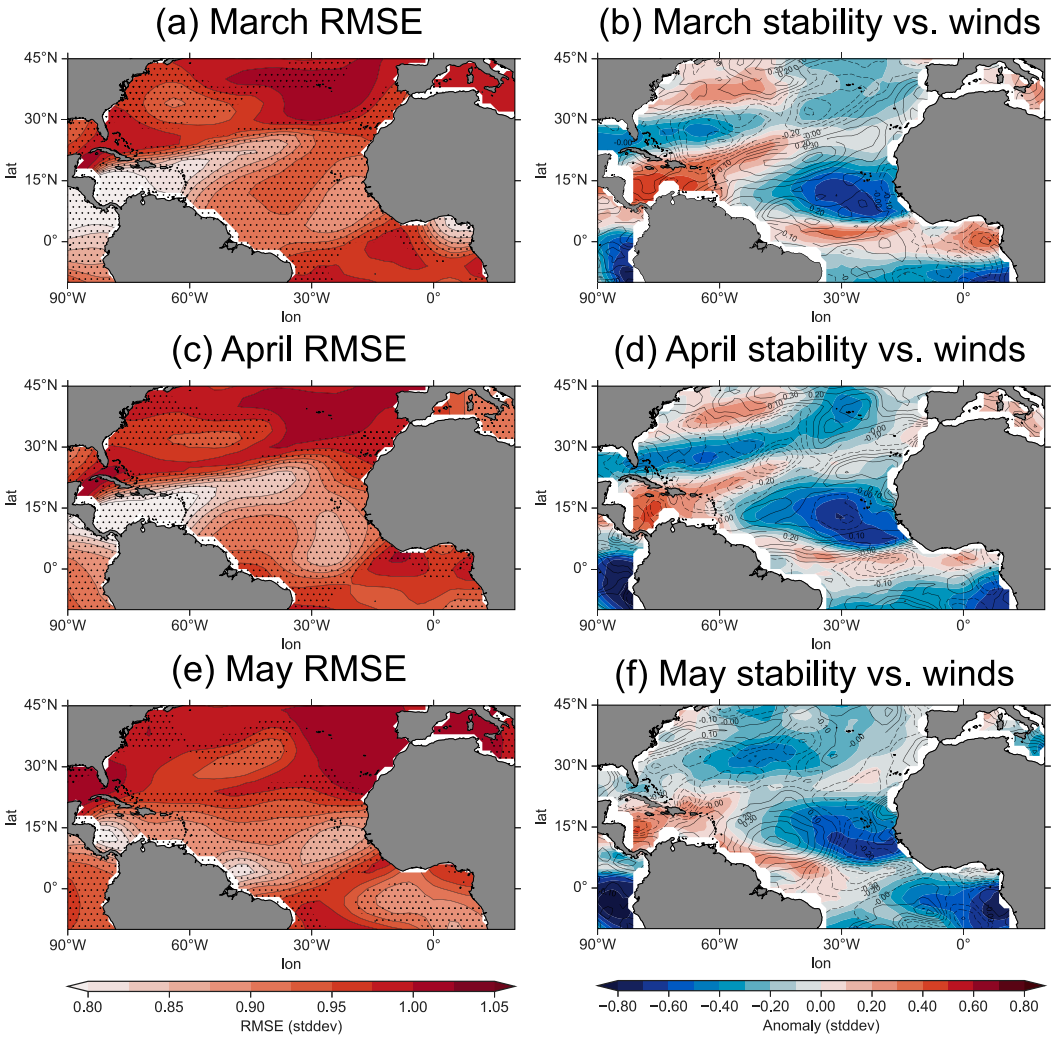

FIG. 4. Linearity vs SST contributions. (left) RMSE maps between the ONDJF Niño-3.4 index and SST and pointwise multiple linear regression coefficients of tropospheric stability (shading) and (right) 950 hPa total winds (contours) against the SST for (top) March, (middle) April, and (bottom) May. Stippling in RMSE maps represents statistical significance at the 95% level by using a two-tailed *t* test. Note that the color bar for the RMSE maps is not spaced linearly.

static stability peaks in the Caribbean, suggesting that the Caribbean SST anomalies are driven by static stability, while trade wind anomalies drive central TNA SST anomalies. The spatial distribution also matches the lower-tropospheric stability composites found in Fig. S4.

In the central TNA region (10°N, 45°W), the linearity decreases, as seen by higher RMSE values. This lower linearity region tilts from southwest to the northeast (Fig. 4a). Comparing this area to March's MLR map (Fig. 4b), the decrease in linearity corresponds to where influences from stability are minimal. This overlap suggests that less linear areas are associated with wind anomalies and that the static stability's influence on the SST is more linear.

Comparing RMSE maps (Figs. 4a,c,e) and the SST composites (Fig. 2) confirms that high linearity in the Caribbean, deep tropics, and West African coast corresponds with consistently large SST anomalies in the composites, as expected. This suggests that previous patterns described in the SST composites are strongly influenced by static stability and wind anomalies, where the former is more linear than the latter.

The spatial distribution of the May RMSE and extreme El Niño SST composite also resemble each other (Figs. 2j and 4e), including the two centers on either side of the equator. These two centers are likely the result of the TNA SSTA intensifying the cross-equatorial temperature gradient, inducing a meridional flow, and triggering a northward shift of the ITCZ (Chiang et al. 2001) (also see Figs. S4c,f). As the ITCZ shifts, it further sustains the interhemispheric flow of surface winds (Chiang 2002). As a result, this meridional flow decreases trade winds in the Northern Hemisphere and increases them in the Southern Hemisphere, explaining the equator's two SSTA centers. Since an intensification of the cross-equatorial SST gradient triggers

the ITCZ displacement, this may explain why the two centers intensify in May instead of in March. As the Atlantic Niño occurs in the southern region of the RMSE maps, this interannual mode of variability likely influences the relationship (Lübbecke et al. 2018). We further break down the relationship with the ITCZ in the following section.

MLR results in the deep tropics show a contrast to the Caribbean (Figs. 4b,d,f). One key factor consists of the differences in static stability anomalies, which affect vertical motion, thereby modifying evaporative cooling and surface shortwave radiation, both of which can induce SST anomalies. Unlike the Caribbean, where increased stability is associated with an increase in SSTs, the deep tropics SSTs are negatively correlated between SST and stability. These differences could be explained by the complex differences between the Caribbean and deep tropics (south of 10°N, Czaja et al. 2002). Anomalous meridional shifts of the ITCZ will acutely influence the deep tropics, while the temperature anomaly that propagates from the Pacific to the Atlantic reaches a peak in the subtropics around 20°–30°N. This interplay translates to the Caribbean SST being positively correlated with static stability, as the atmospheric temperature anomaly surpasses any opposing influence on stability, such as from the Hadley Cell. Over the deep tropics, the temperature anomaly is less robust, while the influence from the ITCZ on vertical motion increases, making stability influences less robust overall (as seen by lack of statistical significance in Fig. S4).

c. *Tropical mechanisms*

To examine the tropical pathway, we separate it into the secondary Gill and TT indices. The seasonal evolution of the respective indices is shown in Figs. 5a and 5b, while Figs. 5c and 5d show the respective peak months of each index, that is, JFM for the secondary Gill index, and February to April (FMA) for the TT index, using the rolling ONDJF Niño-3.4 method.

During secondary Gill mechanism peak (JFM) (Fig. 5c), the mechanism consistently increases in strength with respect to Niño-3.4 SSTA, from strong La Niña to extreme El Niño events. Overall, the secondary Gill mechanism cannot explain the plateau during El Niño; rather, the tropical contribution to the pathway leads to an increase in TNA SSTA during extreme El Niño (Fig. 5c).

As the TT mechanism peaks in FMA (Fig. 5b), moderate and strong El Niño events show little difference. This also occurs for La Niña events. By considering only the peak month, we show that the index follows the linear fit. Furthermore, the variability is higher than the secondary Gill index. Unlike for the secondary Gill index, plateau slightly for strong La Niña events, where little increase occurs for La Niña events past the −1.5 to −1.0 std dev bin. Overall, both pathways are relatively linear, although more so for the secondary Gill mechanism. The TT index result is consistent with Su et al. (2003), and Lin et al. (2007), who also found that the TT mechanism is linear.

As the interhemispheric temperature gradient in the tropical Atlantic grows, favoring a northward shift of the ITCZ in boreal spring, this can play an important role in reinforcing or creating deep tropic trade wind anomalies. Furthermore, Jiang and Li (2019) found that this shift may contribute more to the trade wind anomaly in the deep tropics than the secondary Gill mechanism. We, therefore, investigate the linearity of the ITCZ shift using the first MCA mode between the precipitation and 950 hPa meridional wind fields (Fig. 6). We use meridional winds, as they correspond closely to cross-equatorial winds and associated meridional shift of the ITCZ. The first mode captures 24.3% of covariance between these two fields. As expected from past studies, the homogeneous maps (Figs. 6a,b) indicate that a northward displacement of the ITCZ is associated with northward cross-equatorial winds in the tropical Atlantic.

Seasonal evolution of the PCs for precipitation and meridional wind fields are shown in Figs. 6c and 6d. The ITCZ peak occurs between April and June (AMJ), while meridional winds peak around one month earlier, in MAM. This is consistent with Chiang et al. (2001), who showed that the meridional wind anomaly drives the ITCZ shift. It is also consistent with Richter et al. (2017), who describes the phase locking of the ITCZ and equatorial wind anomalies. These peak months are also plotted in Figs. 6e and 6f for the associated PCs of each field using a rolling ONDJF Niño-3.4 index (similar to Fig. 5).

Results of using a rolling ONDJF Niño-3.4 index show that both the ITCZ anomaly, and associated meridional winds follow a linear fit. The extreme endpoints do not deviate from this relationship, as previously seen for the TT mechanism. They show a much larger variability about the linear fit, but residuals are randomly distributed. This higher variability can be explained by the fact that the Atlantic Ocean has the flattest meridional temperature profile during boreal spring, causing the ITCZ to be sensitive to slight differences in SST anomalies (Chiang 2002). Overall, the linearity confirms that the ITCZ response over the Atlantic is linear with ENSO and does not contribute to the TNA SSTA plateau for El Niño events.

d. *Extratropical pathway*

Next, we analyze the teleconnection through the extratropics. Anomalies can project onto the PNA pattern and Pacific–South American (PSA) pattern. Since the latter's influence focuses primarily on the South Atlantic (Rodrigues et al. 2015), we focus on the PNA (Mo and Paegle 2001) (Fig. 12). Past studies show that the PNA consists of both linear and nonlinear aspects. For example, the Aleutian low, which is the northwestern low pressure region of the PNA, is nonlinear and unresponsive to increases in ENSO magnitude during La Niña events (Straus and Shukla 2002).

The PNA-related southeastern low located over the United States and western TNA plays an important role in developing the TNA SSTA by influencing the downward motion of the subtropical high over the Atlantic (Hastenrath 2000). To quantify the PNA impact over the subtropical Atlantic, we create a separate index in addition to using the PNA. Since the PNA's influence involves ascending and descending anomalies, we use the area-averaged SLP anomaly over the PNA's southeastern region.

Seasonal evolution (Figs. 7a,b) for both indices peaks around JFM. The ONDJF rolling Niño-3.4 method during JFM (Figs. 7c,d) indicates a similar evolution for both indices. Since

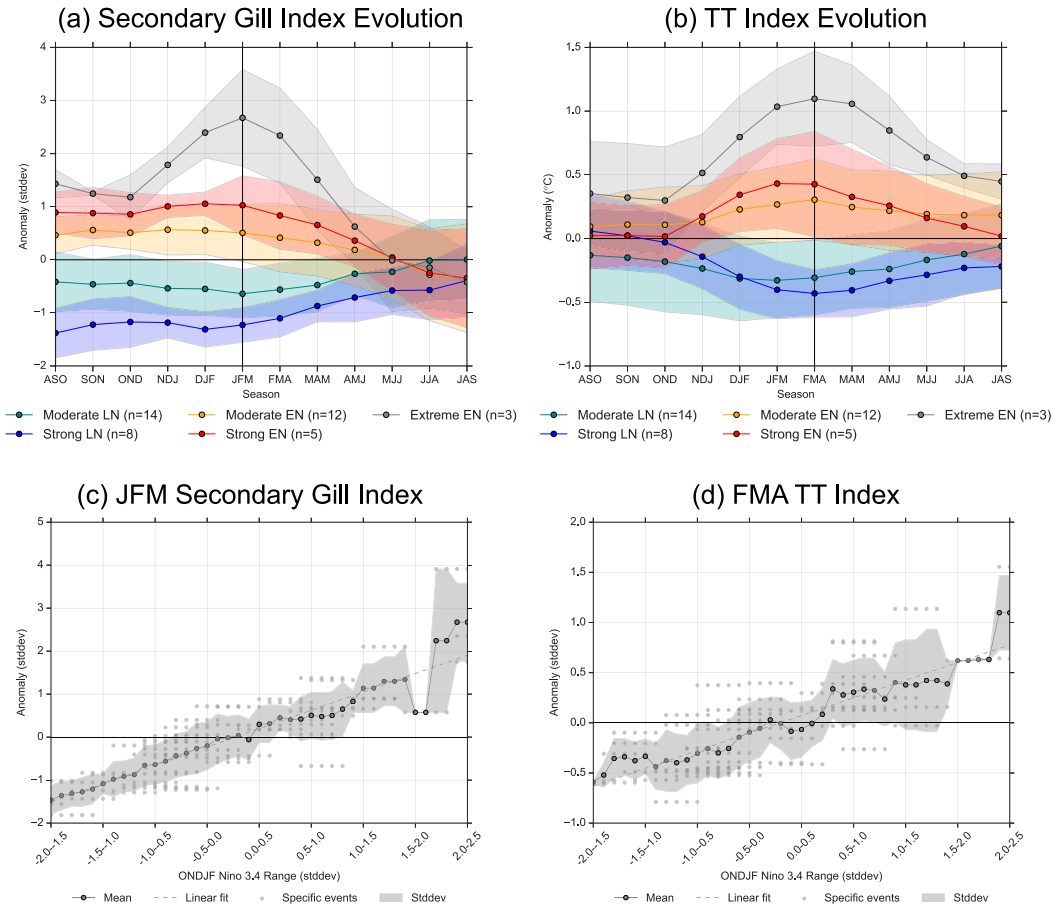

FIG. 5. Tropical pathway evolution. As in Fig. 3, but using the secondary Gill and TT indices.

the southeastern low is a subset region of the PNA, this is to be expected. Furthermore, both the PNA and southeastern low residuals, with respect to a linear fit, are not randomly distributed (Figs. 7c,d), indicating a nonlinear aspect. To investigate this, we analyze the residuals in Fig. 8. To calculate the residuals, we directly compare the southeastern low to the ONDJF Niño-3.4 index to determine a linear regression, with the residuals defined as the difference between the linear fit and southeastern low anomaly (southeastern low minus the linear fit, as seen in Fig. S2f). In doing so, we avoid any smoothing that the rolling ONDJF Niño-3.4 index may produce.

To investigate the source of this nonlinearity, we composite JFM SST and JFM SLP fields during years with a positive residual (>1.0 hPa) and negative residual (<−1.0 hPa) (Figs. 8a–d). The JFM SSTA (Figs. 8a,b) over the Pacific shows a distinct difference between the anomalous SST patterns. Positive residuals are associated with a central Pacific El Niño pattern peaking around the date line, and negative residuals show an eastern Pacific El Niño pattern. Since the southeastern low index is anticorrelated to the Niño-3.4 index, a positive residual weakens the response during an El Niño event, showing eastern El Niño events tend to perturb the TNA region more effectively. This is consistent with Taschetto et al. (2016), who found that the PNA response is stronger for eastern El Niño events, compared to central El Niño. Furthermore, we extend their findings by examining La Niña events. However, since our SST residual composites only show El Niño–like patterns, this says little about residuals during La Niña events.

As the NAO may also modulate the southeastern low, we analyze the SLP during JFM (Figs. 8c,d). Composites show that the residuals positively correlate with the NAO. This connection may have contributed to the oscillation of the residuals for La Niña events. This is because the NAO is negative during moderate La Niña and positive during strong La Niña, matching the residuals (Figs. 2a,c). However, this relationship breaks down for extreme El Niño events, as the NAO is positive, while the residual is negative. This breakdown hints at the interplay between the NAO and ENSO's longitudinal position for modulating the southeastern low, where the NAO plays the dominant role during La Niña events. The results during La Niña may also be less robust than during El Niño, as the structure varies between NAO–like and wave train–like between positive and negative residuals (Figs. S5a,b).

To investigate these patterns, Figs. 8e and 8f show the scatterplots between the residuals and the JFM EMI and JFM NAO indices, respectively. The correlation between the EMI

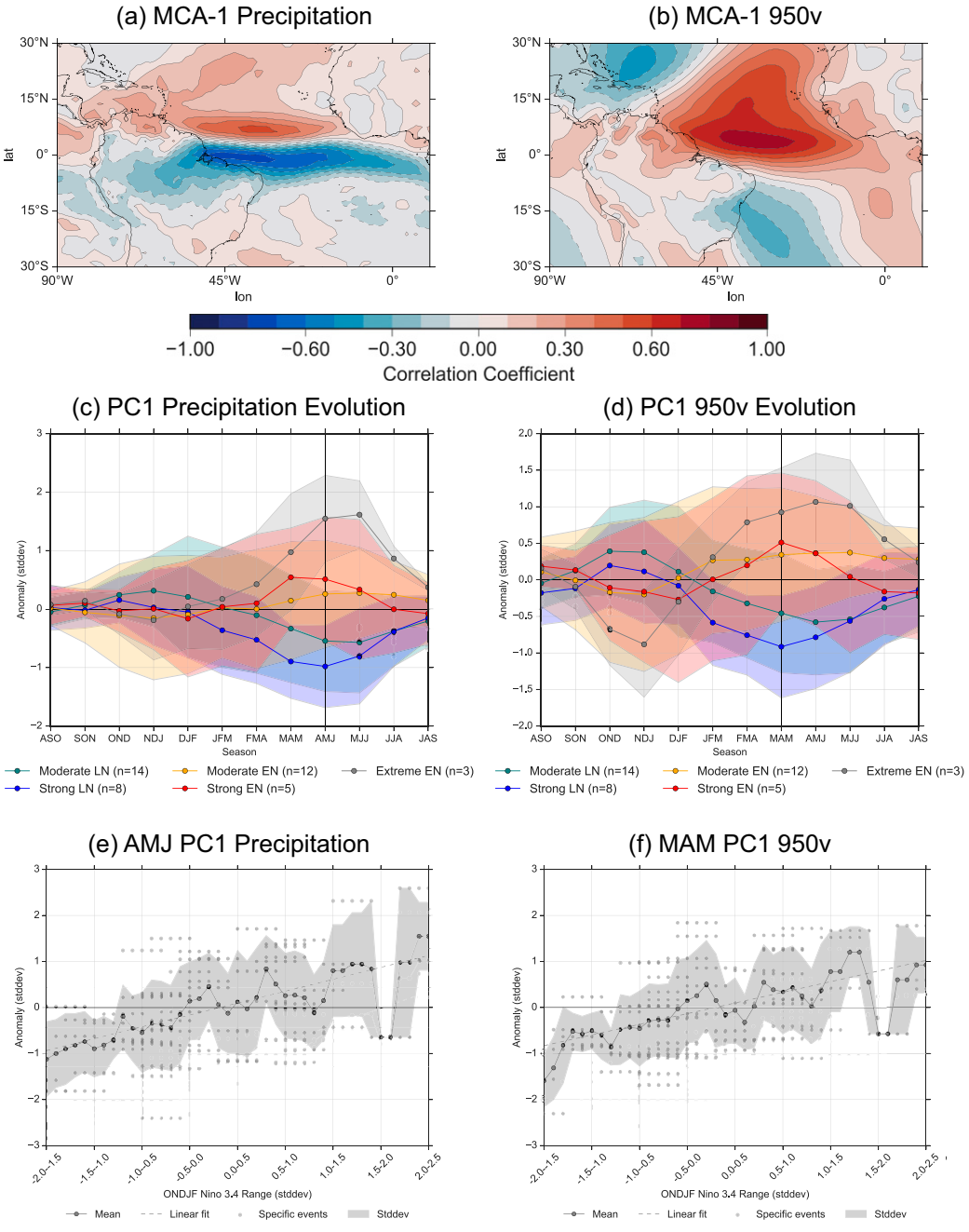

FIG. 6. ITCZ and meridional winds. The homogeneous maps for the first modes of (a) precipitation and (b) 950 hPa meridional winds fields. (c),(d) The corresponding expansion coefficients (PCs) are used to represent the composited evolution following an ENSO event. (e),(f) The expansion coefficients during the peak precipitation (AMJ) and peak meridional winds (MAM), respectively. Note that the *y* axes for (c)–(f) change according to the variable. The MCA includes all months from 1958 until 2016. Vertical lines in (c) and (d) represent the peak of each index.

and all residuals is 0.13, increasing to 0.23 for only El Niño events and decreasing to −0.03 for La Niña events. Conversely, the correlation between all residuals and the NAO is 0.55, changing to 0.58 and 0.38 when considering only El Niño and La Niña events, respectively. This shows that the NAO is a dominant influence during La Niña, while the longitudinal location of the tropical Pacific SSTA is more important during El Niño events. Overall, the NAO and the longitudinal position of

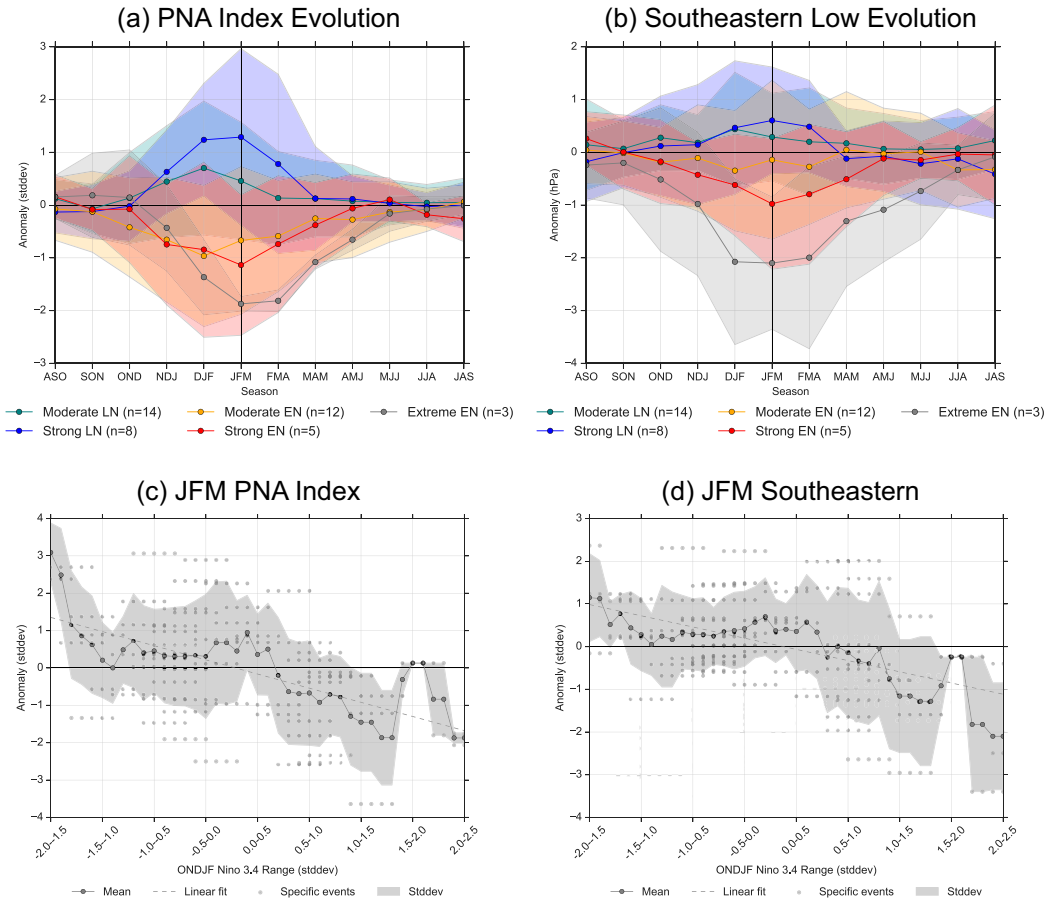

FIG. 7. PNA and southeastern low evolution. As in Fig. 3, but using the first PC of the 200 hPa geopotential height over North America to represent the PNA index and the area averaged sea level pressure over 25°–35°N, 90°–70°E for the southeastern low pressure area of the PNA. Vertical lines in (a) and (b) represent the peak of each index.

the SSTA in the equatorial Pacific modulate ENSO's influence onto the TNA, whereby the southeastern low is externally modulated instead of internally nonlinear (Fig. 12).

e. Comparison of mechanisms

We compute the RMSE for each index for full (−2.0 to 2.5 ONDJF Niño-3.4 index), moderate, and strong binning ranges (see Table 2). The secondary Gill and TT index have a smaller RMSE compared to the other indices, indicating that the tropical pathway is more linear than the extratropical pathway. The RMSE for both indices also increases minimally for strong events compared to moderate events. Overall, this does not explain the nonlinearity seen in the TNA SSTA.

We separate the RMSE for moderate and strong ENSO and compare it to the full time series for the MCA of the cross-equatorial flow and meridional shift of the ITCZ. Figures 6e and 6f showed previously that these indices follow a linear fit with high variability. Table 2 confirms this relationship, as there are relatively minimal changes in RMSE between moderate and strong events. In the southeastern low residual analysis, residuals are negative during strong La Niña, decreasing the ability of strong La Niña events to perturb the TNA. Negative residuals are also present for strong and extreme El Niño, increasing the ability of El Niño to perturb the TNA SSTA. As such, this modulation does not explain the nonlinearity in the TNA SSTA. Overall, as both the tropical and extratropical pathways cannot explain why ENSO and the TNA's relationship is nonlinear, this indicates potentially another mechanism at play apart from these teleconnection pathways.

Correlation between the MAM TNA SSTA residuals (with respect to ONDJF Niño-3.4 index) and the January TNA SSTA is 0.65 (Fig. 9a). Such a high correlation shows the importance of preconditioning for explaining the teleconnection but does not indicate if a certain phase or strength of ENSO is more important for the preconditioning, and there is no reason to believe this would be the case. Consequently, results explain little about why extreme El Niño events plateau in SSTA. To further analyze this, we plot the January SST composites for when the residual as mentioned above is ±0.25°C. Results show the SST-tripole pattern for both cases, where SST anomalies extend from the tropics to the North Atlantic, with three distinct poles. This pattern indicates the NAO is likely

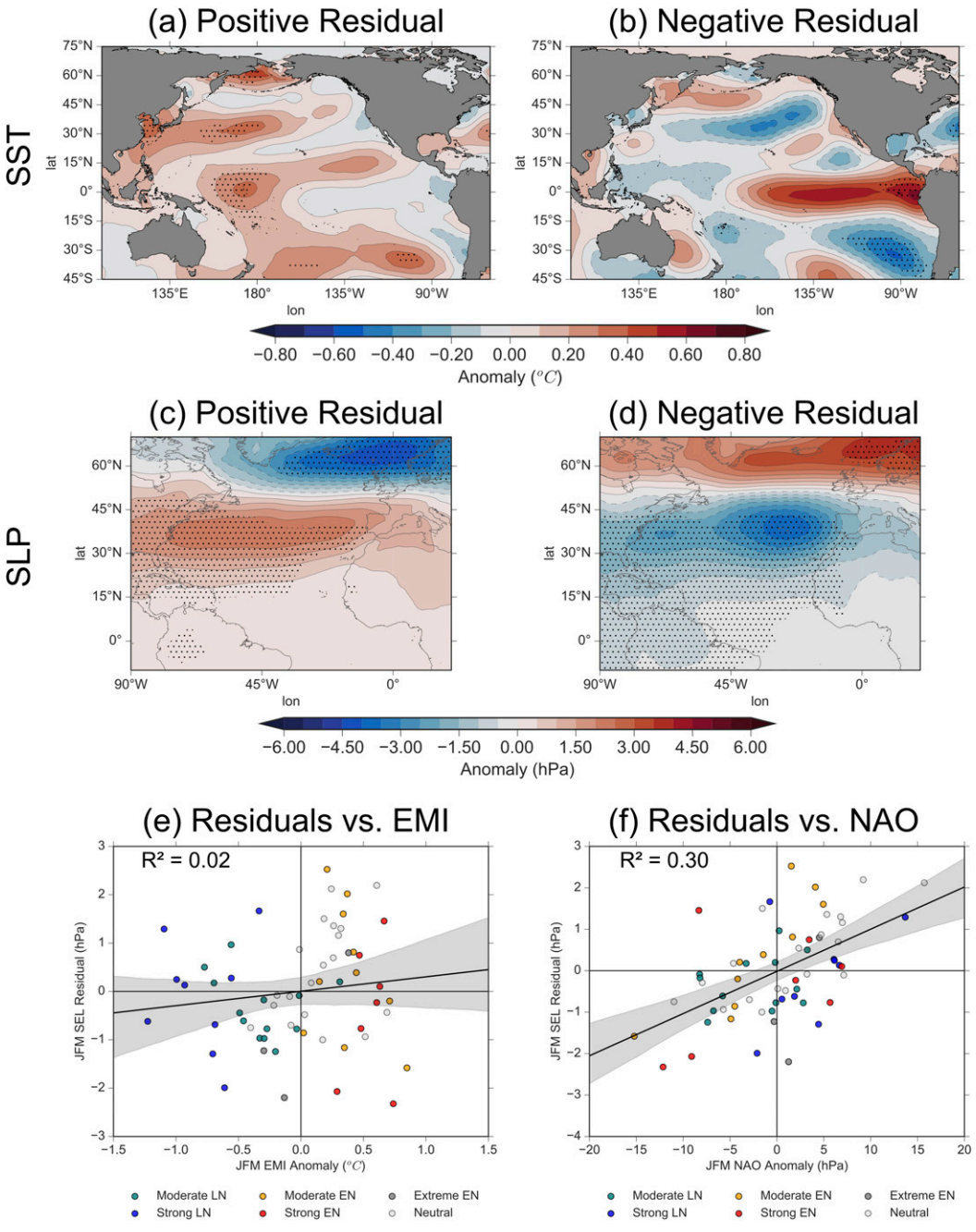

FIG. 8. Relationship between southeastern low, EMI, and NAO. Residuals between the southeastern low and ONDJF Niño-3.4. Residuals were created using a direct comparison between the southeastern low and ONDJF Niño-3.4, where residuals are defined as the difference between the linear regression and southeastern low anomaly. (a),(b) The JFM SST over the Pacific; (c),(d) the JFM SLP over the Atlantic, for positive residuals (>1.0 hPa) and negative residuals (<−1.0 hPa). Years for negative residuals include 1964, 1969, 1971, 1974, 1983, 1987, 1996, 1998, and 2010 and years for positive residuals include 1966, 1988, 1989, 1990, 1994, 1997, 2002, 2004, 2007, 2009, 2015, 2016, 2018, and 2019. (e) The residuals against the JFM EMI index; (f) the residuals against the JFM NAO index. Stippling in (a)–(d) represents statistically significant areas (>95%). Shaded areas in (e) and (f) represent the 95% confidence interval. Correlation between the JFM residuals and JFM EMI and JFM NAO is 0.22 and 0.56, respectively.

TABLE 2. Summary of RMSE values. All values are for normalized indices. Moderate events are defined as ±0.5–1.0 ONDJF Niño-3.4 std dev, and strong events are defined as ±1.0–2.0 ONDJF Niño-3.4 std dev. Months for each index occur during their associated peak month, as seen in previous sections.

Index type	All events	Moderate events	Strong events
Gill	0.561	0.498	0.494
TT	0.629	0.609	0.651
MCA1 precipitation	0.937	0.960	0.879
MCA1 meridional winds	0.856	0.862	0.804
PNA	1.366	1.382	1.300
Southeastern low	1.129	1.042	1.226
TNA	0.850	0.810	0.893

the forcing for the residual SSTA pattern. However, it should be noted that additional external influences or internal variability may be at play.

To explain how the NAO influences the preconditioning differently depending on the ENSO phase and strength, we look to recently discovered asymmetries in the NAO found by Hardiman et al. (2019). They show that an asymmetry in the perturbed NAO occurs between strong El Niño and La Niña, resulting from differences in the tropospheric and stratospheric teleconnection pathway to the North Atlantic. While the tropospheric pathway through the Caribbean is linear with respect to ENSO, the stratospheric pathway fails to grow in strength for a strengthening of the El Niño SSTA. They suggest that this difference in linearity causes the tropospheric pathway, represented by Rossby wave propagation, to dominate during extreme El Niño. As a result, the January NAO anomaly appears as a transatlantic wave pattern during El Niño, which is seen in our extreme El Niño composite patterns (Fig. 2i). The resulting pattern in the North Atlantic acts destructively to the expected trade wind anomaly and may impact SST preconditioning.

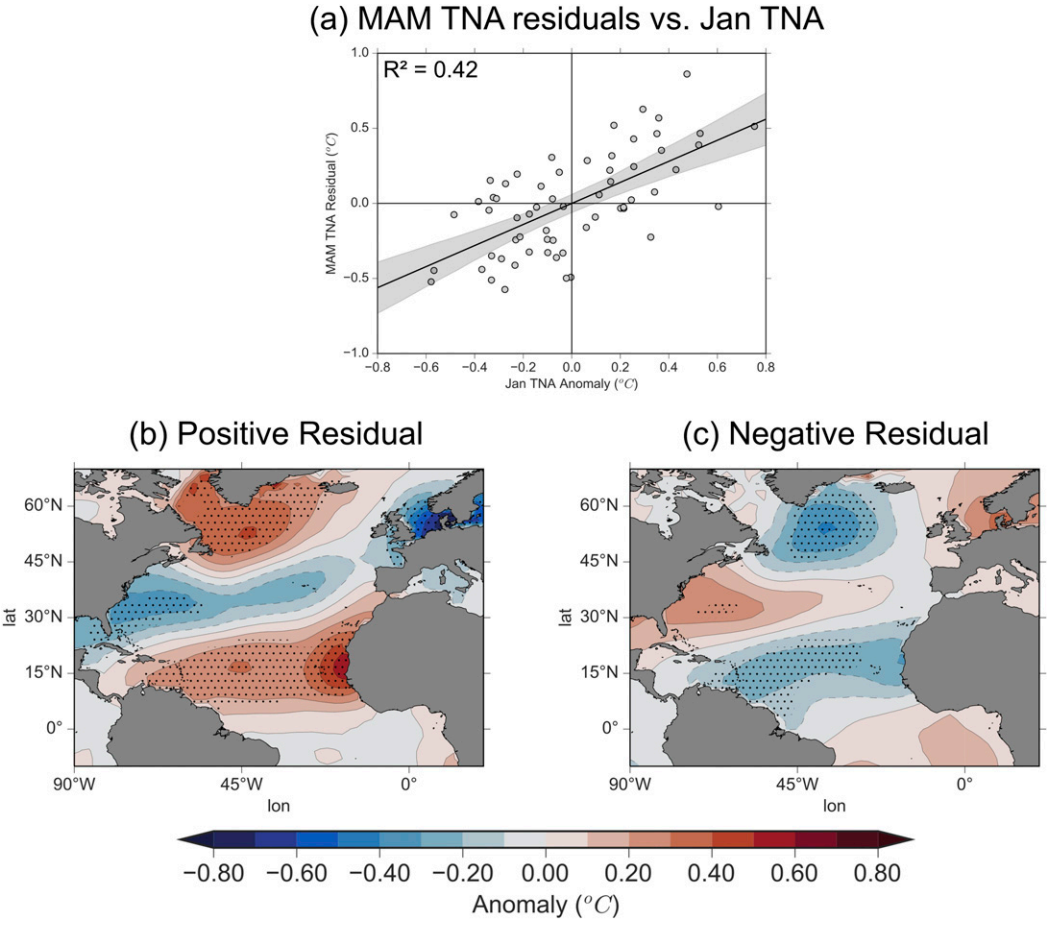

FIG. 9. Residuals analysis for MAM TNA SSTA. (a) Scatterplot between the residual between MAM TNA SSTA and ONDJF Niño-3.4 (without using a rolling range) and the January TNA SSTA. Shaded area represents 95% confidence interval. January SST composite of (b) positive (>0.25°C) and (c) negative (<−0.25°C) residuals between the MAM TNA SST and ONDJF Niño-3.4 (without using a rolling range). Stippling area represents 95% confidence interval using a Monte Carlo analysis.

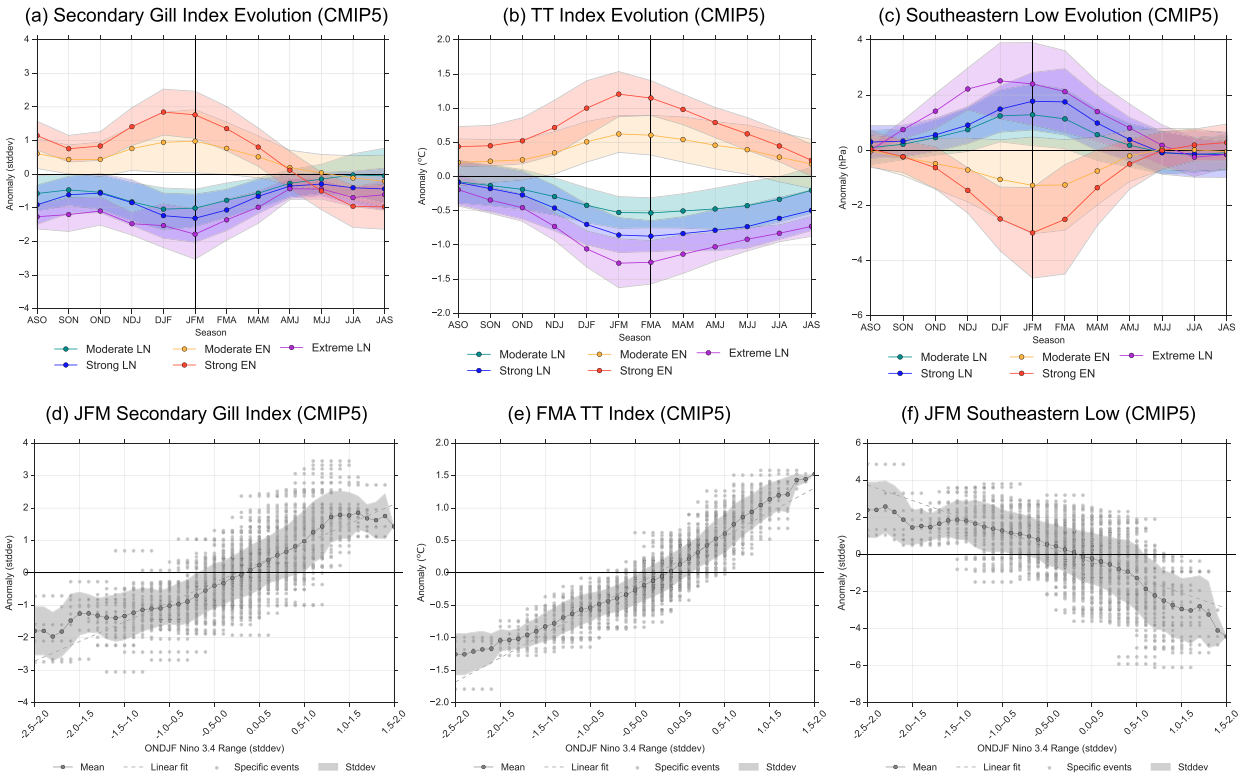

FIG. 10. GFDL CM3 analysis for secondary Gill, TT, and southeastern low. (a)–(c) Composited seasonal evolution; (d)–(f) anomaly for the peak month of each index as a function of the ONDFJ Niño-3.4 range. Bins are defined as in Fig. 3. Vertical lines for (a)–(c) show the JRA-55 peak month, indicating differences in the seasonal evolution between reanalysis and the model.

As opposed to a more zonal NAO pattern, the presence of this wave train shifts the dominant pressure gradient from dominantly meridional to dominantly zonal over the TNA region. By geostrophic balance, this explains why winds shift to primarily meridional, and the lack of strong trade wind anomalies around 20°N. Regions of significant SSTA during extreme El Niño (Fig. 2j), namely the Caribbean and deep tropics, are consistent with static stability changes and a northward shifted ITCZ. The SST dipole in the deep tropics further indicates a positive meridional wind anomaly, which decreases trade winds in the Northern Hemisphere and increases them in the Southern Hemisphere.

f. Comparison with preindustrial model simulation

We evaluate the results in a 500-yr preindustrial simulation of the GFDL CM3. Figures 10a–c shows the TT, secondary Gill, and southeastern low index evolution, while Figs. 10d, 10e, and 10f shows the respective peak month for each index compared to a rolling ONDJF Niño-3.4 method. In comparison to JRA-55, the model is biased toward La Niña events, and extreme El Niño events are absent. The peak months for the model and JRA-55 (represented by a vertical line in Figs. 10a,b,c) show relatively good agreement for moderate events, while strong and extreme subsamples often peaking one season earlier.

Both the secondary Gill and TT indices show a linear behavior until ENSO events approach extreme La Niña (Figs. 10d,e), where the indices begin to plateau. This nonlinearity may reflect the saturation of the atmospheric response to further decreases in SST, as outlined in Jiménez-Esteve and Domeisen (2019). The southeastern low shows similar nonlinear patterns in JRA-55, as seen by negative residuals for both La Niña and El Niño.

The residual analysis (Fig. 11) reveals similar patterns in the Pacific SST and North Atlantic SLP. The positive residual composites show a central El Niño–like pattern (Fig. 11a), with a stronger negative cold tongue in the eastern Pacific. Negative residuals conversely show a strong eastern El Niño–like pattern. Over the North Atlantic, similar patterns emerge, whereby the southeastern low positively correlates with the NAO. This confirms that the influence of the longitudinal position of El Niño and the NAO are key factors for modulating the southeastern low.

4. Summary and conclusions

We study the linearity of all major mechanisms for the ENSO teleconnection to the tropical North Atlantic and their role in the nonlinearity concerning ENSO strength in observed SST over the TNA region. We focus our analysis on reanalysis data, but also compare our results to a preindustrial CMIP5 simulation. We compare the spatial distribution of the deviation from linearity to determine for which areas and for which mechanisms the teleconnection is more linear. We find the

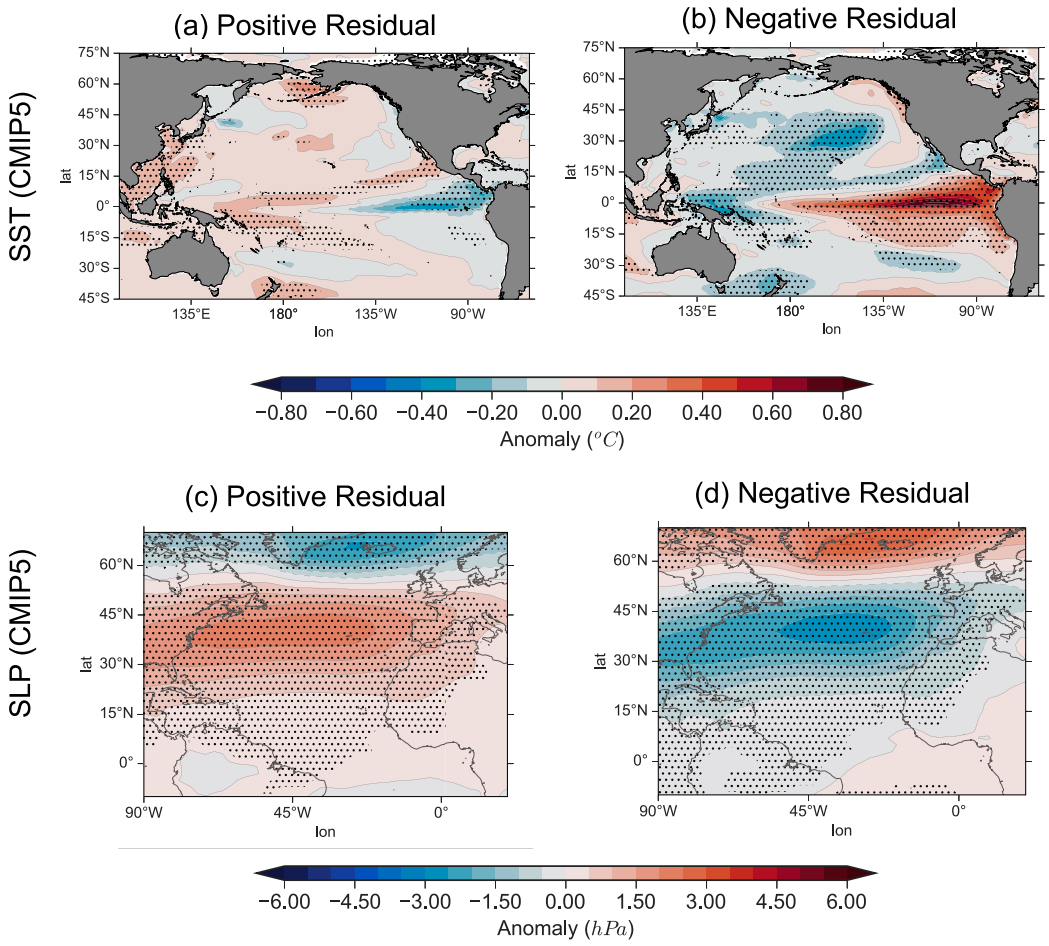

FIG. 11. GFDL CM3 analysis of southeastern low residuals. (a),(b) JFM SSTs over the Pacific and (c),(d) JFM SLP over the Atlantic, for positive residuals (>1.0 hPa) and negative residuals (<−1.0 hPa). Stippling in (a)–(d) represents statistically significant areas (>95%).

deep tropics and Caribbean regions have the most linear relationship with ENSO. Through an MLR analysis we show that these areas are associated with static stability changes and potentially a shift of the ITCZ. Conversely, areas of lower linearity are more strongly associated with wind speed changes.

To investigate each mechanism individually, we divide the teleconnection pathway into tropical and extratropical pathways. We represent the tropical pathway using a secondary Gill index and TT index, while we represent the extratropical pathway with a novel index, called the southeastern low index. The tropical mechanisms respond relatively linearly to changes in ENSO strength, although the TT index exhibits a plateau in strength during strong La Niña events, indicating a potential nonlinearity. This is further confirmed in the model simulation, with the secondary Gill and TT both plateauing in strength during extreme La Niña. The ITCZ movement and cross-equatorial winds respond linearly to changes in Niño-3.4 SSTA, but with high variability.

This study extends our understanding of the teleconnection of ENSO to the tropical Atlantic by considering both ENSO phases. We find that the southeastern low is likely externally modulated by the longitudinal variance of El Niño and the NAO. For La Niña, since the variability in the longitudinal position of the tropical Pacific SST anomalies is smaller than for El Niño, the dominant modulator is suggested to be the NAO. Modeled residual composites including both central and eastern El Niño–like patterns as well as positive and negative NAO patterns confirm this result.

Results show the TNA SSTA nonlinearity is not caused by nonlinearities in the teleconnections themselves but by external factors. These include the NAO and its constructive or destructive interaction with the trade winds and asymmetries in the NAO arise during extreme El Niño. Another potential modulator is the TNA SST preconditioning, which can be related to the NAO. Either modulator can dominate over the other depending on the year. For example, in moderate La Niña years, the NAO acts destructively toward the expected trade wind anomaly and may explain the lack of large SST anomalies. Conversely, during strong El Niño years, the NAO is constructive for expected trade wind anomalies, and the overall trade wind anomaly is strong, but there is a lack of statistically significant SST anomalies. In this case, the preconditioning may play an

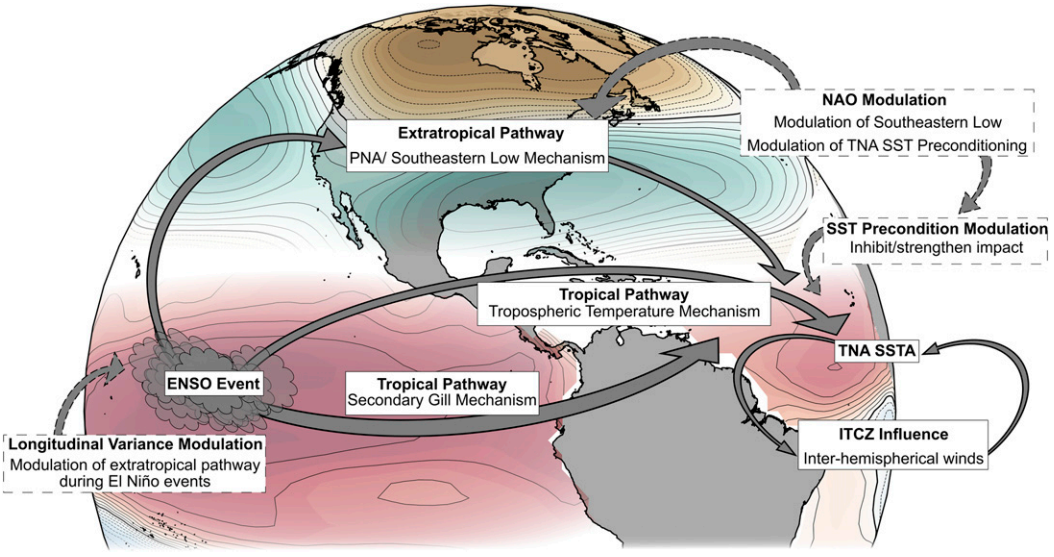

FIG. 12. Schematic of main mechanisms for the ENSO teleconnection toward the tropical Atlantic, as discussed in the text. Shading represents two SVDs between (Pacific SST, Atlantic SST) and (Pacific SST, North American 500 hPa geopotential height), and is used to plot the ENSO SST, TNA SST, and PNA. For the Pacific SST, both SVDs had the same pattern. Dashed arrows and boxes represent modulating factors, while solid arrows and boxes represent the main mechanisms for the teleconnection.

important role, as the strong El Niño has neutral to negative SST preconditioning.

We introduce a novel method to interpret the linearity of the teleconnection by using a rolling ONDJF Niño-3.4 range. Pointwise application over the Atlantic indicates the spatial distribution of the deviation from linearity. However, even as this offers additional statistical interpretations, using reanalysis data alone has clear limitations as there are few extreme El Niño events and no extreme La Niña events.

Finally, this study shows the nontrivial nature of the ENSO teleconnection to the tropical North Atlantic, indicating the need to incorporate additional aspects for more accurate predictions of the TNA SSTA evolution. These aspects include the longitudinal variance, TNA preconditioning, and the NAO, as summarized in Fig. 12. Future studies should look to further our understanding of the respective roles of the longitudinal variability of ENSO and the NAO for modulating the southeastern low, which may differ between La Niña and El Niño.

Acknowledgments. We thank Bernat Jiménez-Esteve, Ole Wulff, and Joke Lübbecke for helpful discussions of the preliminary results. We thank Urs Beyerle for archiving the CMIP5 data at ETH Zurich. The work of J.C. is funded through ETH Grant ETH-17 18-1. Funding from the Swiss National Science Foundation to D.D. through project PP00P2_170523 is gratefully acknowledged. A.S.T. is supported by the Australian Research Council FT160100495. The authors thank three anonymous reviewers and the editor Isla R. Simpson for their careful reading of the manuscript and helpful feedback.

Data availability statement. The JRA-55 and the ERSSTv4 datasets were downloaded through the NCAR research data archive (https://rda.ucar.edu/). The CMIP5 data are available through the Lawrence Livermore National Laboratory (https://esgf-node.llnl.gov/projects/esgf-llnl/).

REFERENCES

Alexander, M. A., I. Bladé, M. Newman, J. R. Lanzante, N.-C. Lau, and J. D. Scott, 2002: The atmospheric bridge: The influence of ENSO teleconnections on air–sea interaction over the global oceans. *J. Climate*, **15**, 2205–2231, https://doi.org/10.1175/1520-0442(2002)015<2205:TABTIO>2.0.CO;2.

Amaya, D. J., and G. R. Foltz, 2014: Impacts of canonical and Modoki El Niño on tropical Atlantic SST. *J. Geophys. Res. Oceans*, **119**, 777–789, https://doi.org/10.1002/2013JC009476.

——, M. J. DeFlorio, A. J. Miller, and S. P. Xie, 2017: WES feedback and the Atlantic meridional mode: Observations and CMIP5 comparisons. *Climate Dyn.*, **49**, 1665–1679, https://doi.org/10.1007/s00382-016-3411-1.

Ashok, K., S. K. Behera, S. A. Rao, H. Weng, and T. Yamagata, 2007: El Niño Modoki and its possible teleconnection. *J. Geophys. Res.*, **112**, C11007, https://doi.org/10.1029/2006JC003798.

Barreto, N. J., M. Mesquita, D. Mendes, M. H. Spyrides, G. U. Pedra, and P. S. Lucio, 2017: Maximum covariance analysis to identify intraseasonal oscillations over tropical Brazil. *Climate Dyn.*, **49**, 1583–1596, https://doi.org/10.1007/s00382-016-3401-3.

Bretherton, C. S., C. Smith, and J. M. Wallace, 1992: An intercomparison of methods for finding coupled patterns in climate data. *J. Climate*, **5**, 541–560, https://doi.org/10.1175/1520-0442(1992)005<0541:AIOMFF>2.0.CO;2.

Brönnimann, S., 2007: Impact of El Niño–Southern Oscillation on European climate. *Rev. Geophys.*, **45**, RG3003, https://doi.org/10.1029/2006RG000199.

Cassou, C., and L. Terray, 2001: Oceanic forcing of the wintertime low-frequency atmospheric variability in the North Atlantic European sector: A study with the ARPEGE model.

J. Climate, **14**, 4266–4291, https://doi.org/10.1175/1520-0442(2001)014<4266:OFOTWL>2.0.CO;2.

Chang, P., Y. Fang, R. Saravanan, L. Ji, and H. Seidel, 2006: The cause of the fragile relationship between the Pacific El Niño and the Atlantic Niño. *Nature*, **443**, 324–328, https://doi.org/10.1038/nature05053.

Chiang, J. C. H., 2002: Deconstructing Atlantic intertropical convergence zone variability: Influence of the local cross-equatorial sea surface temperature gradient and remote forcing from the eastern equatorial Pacific. *J. Geophys. Res.*, **107**, 4004, https://doi.org/10.1029/2000JD000307.

——, and A. H. Sobel, 2002: Tropical tropospheric temperature variations caused by ENSO and their influence on the remote tropical climate. *J. Climate*, **15**, 2616–2631, https://doi.org/10.1175/1520-0442(2002)015<2616:TTTVCB>2.0.CO;2.

——, and D. J. Vimont, 2004: Analogous Pacific and Atlantic meridional modes of tropical atmosphere–ocean variability. *J. Climate*, **17**, 4143–4158, https://doi.org/10.1175/JCLI4953.1.

——, and B. R. Lintner, 2005: Mechanisms of remote tropical surface warming during El Niño. *J. Climate*, **18**, 4130–4149, https://doi.org/10.1175/JCLI3529.1.

——, S. E. Zebiak, and M. A. Cane, 2001: Relative roles of elevated heating and surface temperature gradients in driving anomalous surface winds over tropical oceans. *J. Atmos. Sci.*, **58**, 1371–1394, https://doi.org/10.1175/1520-0469(2001)058<1371:RROEHA>2.0.CO;2.

Czaja, A., P. van der Vaart, and J. Marshall, 2002: A diagnostic study of the role of remote forcing in tropical Atlantic variability. *J. Climate*, **15**, 3280–3290, https://doi.org/10.1175/1520-0442(2002)015<3280:ADSOTR>2.0.CO;2.

Enfield, D. B., and D. A. Mayer, 1997: Tropical Atlantic sea surface temperature variability and its relation to El Niño–Southern Oscillation. *J. Geophys. Res. Oceans*, **102**, 929–945, https://doi.org/10.1029/96JC03296.

Feng, J., T. Lian, J. Ying, J. Li, and G. Li, 2020: Do CMIP5 models show El Niño diversity? *J. Climate*, **33**, 1619–1641, https://doi.org/10.1175/JCLI-D-18-0854.1.

García-Serrano, J., C. Cassou, H. Douville, A. Giannini, and F. J. Doblas-Reyes, 2017: Revisiting the ENSO teleconnection to the tropical North Atlantic. *J. Climate*, **30**, 6945–6957, https://doi.org/10.1175/JCLI-D-16-0641.1.

George, S. E., and M. A. Saunders, 2001: North Atlantic Oscillation impact on tropical North Atlantic winter atmospheric variability. *Geophys. Res. Lett.*, **28**, 1015–1018, https://doi.org/10.1029/2000GL012449.

Giannini, A., R. Saravanan, and P. Chang, 2004: The preconditioning role of tropical Atlantic variability in the development of the ENSO teleconnection: Implications for the prediction of Nordeste rainfall. *Climate Dyn.*, **22**, 839–855, https://doi.org/10.1007/s00382-004-0420-2.

Graf, H. F., and D. Zanchettin, 2012: Central Pacific El Niño, the ''subtropical bridge,'' and Eurasian climate. *J. Geophys. Res.*, **117**, D01102, https://doi.org/10.1029/2011JD016493.

Hardiman, S. C., N. J. Dunstone, A. A. Scaife, D. M. Smith, S. Ineson, J. Lim, and D. Fereday, 2019: The impact of strong El Niño and La Niña events on the North Atlantic. *Geophys. Res. Lett.*, **46**, 2874–2883, https://doi.org/10.1029/2018GL081776.

Hastenrath, S., 2000: Interannual and longer-term variability of upper air circulation in the Northeast Brazil–tropical Atlantic sector. *J. Geophys. Res.*, **105**, 7327–7335, https://doi.org/10.1029/1999JD901104.

Horel, J. D., and J. M. Wallace, 1981: Planetary-scale atmospheric phenomena associated with the Southern Oscillation. *Mon. Wea. Rev.*, **109**, 813–829, https://doi.org/10.1175/1520-0493(1981)109<0813:PSAPAW>2.0.CO;2.

Huang, B., 2002: The ENSO effect on the tropical Atlantic variability: A regionally coupled model study. *Geophys. Res. Lett.*, **29**, 2039, https://doi.org/10.1029/2002GL014872.

——, and Coauthors, 2015: Extended reconstructed sea surface temperature version 4 (ERSST.v4). Part I: Upgrades and intercomparisons. *J. Climate*, **28**, 911–930, https://doi.org/10.1175/JCLI-D-14-00006.1.

Izumo, T., and Coauthors, 2010: Influence of the state of the Indian Ocean dipole on the following years El Niño. *Nat. Geosci.*, **3**, 168–172, https://doi.org/10.1038/ngeo760.

Jiang, L., and T. Li, 2019: Relative roles of El Niño-induced extratropical and tropical forcing in generating tropical North Atlantic (TNA) SST anomaly. *Climate Dyn.*, **53**, 3791–3804, https://doi.org/10.1007/s00382-019-04748-7.

Jiménez-Esteve, B., and D. I. Domeisen, 2018: The tropospheric pathway of the ENSO–North Atlantic teleconnection. *J. Climate*, **31**, 4563–4584, https://doi.org/10.1175/JCLI-D-17-0716.1.

——, and ——, 2019: Nonlinearity in the North Pacific atmospheric response to a linear ENSO forcing. *Geophys. Res. Lett.*, **46**, 2271–2281, https://doi.org/10.1029/2018GL081226.

Klein, S. A., and D. L. Hartmann, 1993: The seasonal cycle of low stratiform clouds. *J. Climate*, **6**, 1587–1606, https://doi.org/10.1175/1520-0442(1993)006<1587:TSCOLS>2.0.CO;2.

——, B. J. Soden, and N.-C. Lau, 1999: Remote sea surface temperature variations during ENSO: Evidence for a tropical atmospheric bridge. *J. Climate*, **12**, 917–932, https://doi.org/10.1175/1520-0442(1999)012<0917:RSSTVD>2.0.CO;2.

Kobayashi, S., and Coauthors, 2015: The JRA-55 reanalysis: General specifications and basic characteristics. *J. Meteor. Soc. Japan*, **93**, 5–48, https://doi.org/10.2151/jmsj.2015-001.

Lau, N.-C., and M. J. Nath, 1996: The role of the ''atmospheric bridge'' in linking tropical Pacific ENSO events to extratropical SST anomalies. *J. Climate*, **9**, 2036–2057, https://doi.org/10.1175/1520-0442(1996)009<2036:TROTBI>2.0.CO;2.

Lee, J. Y., B. Wang, K. H. Seo, J. S. Kug, Y. S. Choi, Y. Kosaka, and K. J. Ha, 2014: Future change of Northern Hemisphere summer tropical–extratropical teleconnection in CMIP5 models. *J. Climate*, **27**, 3643–3664, https://doi.org/10.1175/JCLI-D-13-00261.1.

Lee, S.-K., D. B. Enfield, and C. Wang, 2008: Why do some El Niños have no impact on tropical North Atlantic SST? *Geophys. Res. Lett.*, **35**, L16705, https://doi.org/10.1029/2008GL034734.

Li, J., and J. X. Wang, 2003: A new North Atlantic Oscillation index and its variability. *Adv. Atmos. Sci.*, **20**, 661–676, https://doi.org/10.1007/BF02915394.

Lin, H., J. Derome, and G. Brunet, 2007: The nonlinear transient atmospheric response to tropical forcing. *J. Climate*, **20**, 5642–5665, https://doi.org/10.1175/2007JCLI1383.1.

Lübbecke, J. F., B. Rodríguez-Fonseca, I. Richter, M. Martín-Rey, T. Losada, I. Polo, and N. S. Keenlyside, 2018: Equatorial Atlantic variability—Modes, mechanisms, and global teleconnections. *Wiley Interdiscip. Rev.: Climate Change*, **9**, e527, https://doi.org/10.1002/wcc.527.

Maldonado, T., A. Rutgersson, J. Amador, E. Alfaro, and B. Claremar, 2016: Variability of the Caribbean low-level jet

during boreal winter: Large-scale forcings. *Int. J. Climatol.*, **36**, 1954–1969, https://doi.org/10.1002/joc.4472.

Mathieu, P. P., R. T. Sutton, B. Dong, and M. Collins, 2004: Predictability of winter climate over the North Atlantic European region during ENSO events. *J. Climate*, **17**, 1953–1974, https://doi.org/10.1175/1520-0442(2004)017<1953:POWCOT>2.0.CO;2.

Mc Shine, N. D., R. M. Clarke, S. Gualdi, A. Navarra, and X. T. Chadee, 2019: Influences of the Atlantic and Pacific Oceans on rainy season precipitation for the southernmost Caribbean small island state, Trinidad. *Atmosphere*, **10**, 707, https://doi.org/10.3390/atmos10110707.

Miller, R. L., 1997: Tropical thermostats and low cloud cover. *J. Climate*, **10**, 409–440, https://doi.org/10.1175/1520-0442(1997)010<0409:TTALCC>2.0.CO;2.

Mo, K. C., and J. N. Paegle, 2001: The Pacific–South American modes and their downstream effects. *Int. J. Climatol.*, **21**, 1211–1229, https://doi.org/10.1002/joc.685.

Nobre, P., and J. Shukla, 1996: Variations of sea surface temperature, wind stress, and rainfall over the tropical Atlantic and South America. *J. Climate*, **9**, 2464–2479, https://doi.org/10.1175/1520-0442(1996)009<2464:VOSSTW>2.0.CO;2.

Noreen, E. W., 1990: *Computer-Intensive Methods for Testing Hypotheses: An Introduction*. Wiley, 229 pp.

Riaz, S. M. F., M. J. Iqbal, and M. J. Baig, 2018: Influence of Siberian high on temperature variability over northern areas of South Asia. *Meteor. Atmos. Phys.*, **130**, 441–457, https://doi.org/10.1007/s00703-017-0531-z.

Richter, I., S. P. Xie, Y. Morioka, T. Doi, B. Taguchi, and S. Behera, 2017: Phase locking of equatorial Atlantic variability through the seasonal migration of the ITCZ. *Climate Dyn.*, **48**, 3615–3629, https://doi.org/10.1007/s00382-016-3289-y.

Robinson, W. A., S. Li, and S. Peng, 2003: Dynamical nonlinearity in the atmospheric response to Atlantic sea surface temperature anomalies. *Geophys. Res. Lett.*, **30**, 2038, https://doi.org/10.1029/2003GL018416.

Rodrigues, R. R., and M. J. McPhaden, 2014: Why did the 2011–2012 la Niña cause a severe drought in the Brazilian Northeast? *Geophys. Res. Lett.*, **41**, 1012–1018, https://doi.org/10.1002/2013GL058703.

——, R. J. Haarsma, E. J. Campos, and T. Ambrizzi, 2011: The impacts of inter–El Niño variability on the tropical Atlantic and northeast Brazil climate. *J. Climate*, **24**, 3402–3422, https://doi.org/10.1175/2011JCLI3983.1.

——, E. J. Campos, and R. Haarsma, 2015: The impact of ENSO on the South Atlantic subtropical dipole mode. *J. Climate*, **28**, 2691–2705, https://doi.org/10.1175/JCLI-D-14-00483.1.

Saravanan, R., and P. Chang, 2000: Interaction between tropical Atlantic variability and El Nino–Southern Oscillation. *J. Climate*, **13**, 2177–2194, https://doi.org/10.1175/1520-0442(2000)013<2177:IBTAVA>2.0.CO;2.

Sasaki, W., T. Doi, K. J. Richards, and Y. Masumoto, 2014a: Impact of the equatorial Atlantic sea surface temperature on the tropical Pacific in a CGCM. *Climate Dyn.*, **43**, 2539–2552, https://doi.org/10.1007/s00382-014-2072-1.

——, ——, ——, and ——, 2014b: The influence of ENSO on the equatorial Atlantic precipitation through the Walker circulation in a CGCM. *Climate Dyn.*, **44**, 191–202, https://doi.org/10.1007/s00382-014-2133-5.

Servain, J., I. Wainer, J. P. McCreary, and A. Dessier, 1999: Relationship between the equatorial and meridional modes of climatic variability in the tropical Atlantic. *Geophys. Res. Lett.*, **26**, 485–488, https://doi.org/10.1029/1999GL900014.

Sobel, A. H., I. M. Held, and C. S. Bretherton, 2002: The ENSO signal in tropical tropospheric temperature. *J. Climate*, **15**, 2702–2706, https://doi.org/10.1175/1520-0442(2002)015<2702:TESITT>2.0.CO;2.

Straus, D. M., and J. Shukla, 2002: Does ENSO force the PNA? *J. Climate*, **15**, 2340–2358, https://doi.org/10.1175/1520-0442(2002)015<2340:DEFTP>2.0.CO;2.

Su, H., J. D. Neelin, and J. E. Meyerson, 2003: Sensitivity of tropical tropospheric temperature to sea surface temperature forcing. *J. Climate*, **16**, 1283–1301, https://doi.org/10.1175/1520-0442-16.9.1283.

Sutton, R. T., W. A. Norton, and S. P. Jewson, 2000: The North Atlantic Oscillation—What role for the ocean? *Atmos. Sci. Lett.*, **1**, 89–100, https://doi.org/10.1006/asle.2000.0018.

Taschetto, A. S., A. S. Gupta, N. C. Jourdain, A. Santoso, C. C. Ummenhofer, and M. H. England, 2014: Cold tongue and warm pool ENSO events in CMIP5: Mean state and future projections. *J. Climate*, **27**, 2861–2885, https://doi.org/10.1175/JCLI-D-13-00437.1.

——, R. R. Rodrigues, G. A. Meehl, S. McGregor, and M. H. England, 2016: How sensitive are the Pacific–tropical North Atlantic teleconnections to the position and intensity of El Niño-related warming? *Climate Dyn.*, **46**, 1841–1860, https://doi.org/10.1007/s00382-015-2679-x.

Vimont, D. J., and J. P. Kossin, 2007: The Atlantic meridional mode and hurricane activity. *Geophys. Res. Lett.*, **34**, L07709, https://doi.org/10.1029/2007GL029683.

Wallace, J. M., and D. S. Gutzler, 1981: Teleconnections in the geopotential height field during the Northern Hemisphere winter. *Mon. Wea. Rev.*, **109**, 784–812, https://doi.org/10.1175/1520-0493(1981)109<0784:TITGHF>2.0.CO;2.

Wang, C., 2004: ENSO, Atlantic climate variability, and the Walker and Hadley circulations. *The Hadley Circulation: Present, Past and Future*, H. F. Diaz and R. S. Bradley, Eds. Springer, 173–202.

——, D. B. Enfield, S. K. Lee, and C. W. Landsea, 2006: Influences of the Atlantic warm pool on Western Hemisphere summer rainfall and Atlantic hurricanes. *J. Climate*, **19**, 3011–3028, https://doi.org/10.1175/JCLI3770.1.

Wanner, H., S. Brönnimann, C. Casty, D. Gyalistras, J. Luterbacher, C. Schmutz, D. B. Stephenson, and E. Xoplaki, 2001: North Atlantic oscillation—Concepts and studies. *Surv. Geophys.*, **22**, 321–381, https://doi.org/10.1023/A:1014217317898.

Whyte, F. S., M. A. Taylor, T. S. Stephenson, and J. D. Campbell, 2008: Features of the Caribbean low level jet. *Int. J. Climatol.*, **28**, 119–128, https://doi.org/10.1002/joc.1510.

Wood, R., and C. S. Bretherton, 2006: On the relationship between stratiform low cloud cover and lower-tropospheric stability. *J. Climate*, **19**, 6425–6432, https://doi.org/10.1175/JCLI3988.1.

Wu, L., F. He, and Z. Liu, 2005: Coupled ocean-atmosphere response to north tropical Atlantic SST: Tropical Atlantic dipole and ENSO. *Geophys. Res. Lett.*, **32**, L21712, https://doi.org/10.1029/2005GL024222.

Wu, R., and Z. He, 2019: Northern tropical Atlantic warming in El Niño decaying spring: Impacts of El Niño amplitude. *Geophys. Res. Lett.*, **46**, 14 072–14 081, https://doi.org/10.1029/2019GL085840.

——, S. Yang, S. Liu, L. Sun, Y. Lian, and Z. Gao, 2011: Northeast China summer temperature and North Atlantic

SST. *J. Geophys. Res.*, **116**, D16116, https://doi.org/10.1029/2011JD015779.

——, M. Lin, and H. Sun, 2020: Impacts of different types of El Niño and La Niña on northern tropical Atlantic sea surface temperature. *Climate Dyn.*, **54**, 4147–4167, https://doi.org/10.1007/s00382-020-05220-7.

Xie, S., and S. G. H. Philander, 1994: A coupled ocean–atmosphere model of relevance to the ITCZ in the eastern Pacific. *Tellus*, **46A**, 340–350, https://doi.org/10.3402/tellusa.v46i4.15484.

Yulaeva, E., and J. M. Wallace, 1994: The signature of ENSO in global temperature and precipitation fields derived from the microwave sounding unit. *J. Climate*, **7**, 1719–1736, https://doi.org/10.1175/1520-0442(1994)007<1719:TSOEIG>2.0.CO;2.

Zhang, W., Z. Wang, M. F. Stuecker, A. G. Turner, F. F. Jin, and X. Geng, 2019: Impact of ENSO longitudinal position on teleconnections to the NAO. *Climate Dyn.*, **52**, 257–274, https://doi.org/10.1007/s00382-018-4135-1.